E86-10004
NASA-CR-176267

CRinc

(E86-10004 NASA-CR-176267) EVALUATION OF SPACE SAR AS A LAND-COVER CLASSIFICATION Final Report. (Kansas Univ. Center for Research, Inc.) 123 p HC A06/MF A01 N86-12740

CSCL 02B G3/43 Unclas 00004

THE UNIVERSITY of KANSAS CENTER for RESEARCH, INC.

2291 Irving Hill Drive-Campus West Lawrence, Kansas 66045

THE UNIVERSITY OF KANSAS CENTER FOR RESEARCH, INC.

2291 Irving Hill Drive—Campus West
Lawrence, Kansas 66045-2969

Telephone: (913) 864-3441

EVALUATION OF SPACE SAR AS A LAND-COVER CLASSIFIER

B. Brisco
F. T. Ulaby
T. H. Lee Williams

Remote Sensing Laboratory
RSL Technical Report 605-1

Supported by:
NATIONAL AERONAUTICS AND SPACE ADMINISTRATION
JOHNSON SPACE CENTER
Houston, Texas 77058
Grant No. NCC9-7

TABLE OF CONTENTS

Page

ABSTRACT iii

LIST OF FIGURES iv

LIST OF TABLES vi

CHAPTER 1 INTRODUCTION 1

1.1 General 1

1.2 Microwave Remote Sensing 2

1.3 The Multidimensional Approach to Remote Sensing 3

1.4 Scope of the Investigation 5

CHAPTER 2 BACKGROUND INFORMATION AND LITERATURE REVIEW 7

2.1 Introduction 7

2.2 Interpretation of Radar Imagery 8

2.3 Land-Cover Mapping with Radar 11

2.4 Forest-Cover Mapping with Radar 15

2.5 Agricultural Discrimination with Radar 19

2.6 Summary 23

CHAPTER 3 LAND-COVER MAPPING IN OKLAHOMA 25

3.1 Introduction 25

3.2 Image Data and Test-Site Description 26

3.3 Methodology 33

3.4 Pixel Classifications 35

3.5 Spatial Averaging and Multisensor Classification 46

3.6 Summary 52

CHAPTER 4 CROP CLASSIFICATION IN KANSAS.....54

4.1 Introduction.....54

4.2 Image Data and Test-Site Description.....55

4.3 Methodology.....56

4.4 Single-Channel Classification.....62

4.5 Multichannel SAR Classification.....70

4.6 Multisensor Classification.....72

4.7 Summary.....78

CHAPTER 5 FOREST MAPPING WITH RADAR.....81

5.1 Introduction.....81

5.2 Test-Site and Forest Descriptions.....83

5.3 Data Analysis.....83

5.4 Results and Discussion.....92

5.5 Summary.....101

CHAPTER 6 CONCLUDING REMARKS.....103

REFERENCES.....107

Abstract

Over the last two decades, the use of microwaves for remote sensing has increased dramatically, and investigations have been conducted into the use of radar remote-sensing techniques for a wide variety of land and ocean applications. The studies reported herein involve multidimensional approaches to the mapping of land cover, crops, and forests. Dimensionality was achieved by (1) using data from sensors such as Landsat to augment Seasat and Shuttle Imaging Radar (SIR) data, (2) using different image features such as tone and texture, and (3) acquiring multidate data. Seasat, Shuttle Imaging Radar (SIR-A), and Landsat data were used both individually and in combination to map land cover in Oklahoma. The results indicated that radar was the best single sensor (72% accuracy) and produced the best sensor combination (97.5% accuracy) for discriminating among five land-cover categories. Multidate Seasat data and a single date of Landsat coverage were then used in a crop-classification study of western Kansas. The highest accuracy for a single channel was achieved using a Seasat scene, which produced a classification accuracy of 67%. Classification accuracy increased to approximately 75% when either a multidate Seasat combination or Landsat data in a multisensor combination was used. The tonal and textural elements of SIR-A data were then used both alone and in combination to classify forests into five categories. Tone outperformed texture as a one-dimensional classifier, producing an accuracy of 75% compared to the 55% to 60% accuracy obtained using textural measures. By combining tone and texture in a multidimensional classifier, accuracies exceeding 90% were achieved. Thus, in all studies, multidimensional approaches improved the classification accuracy achieved using radar data.

LIST OF FIGURES

Page

Figure 3.1 Geographic locations corresponding to the SAR and Landsat images of Oklahoma, with the land-cover-classification study area delineated.....27

Figure 3.2 SIR-A imagery (Nov. 13, 1982) of the Oklahoma land-cover-classification study area.....28

Figure 3.3 Seasat imagery (Aug. 20, Rev. 774) of the Oklahoma land-cover-classification study area.....29

Figure 3.4 Seasat imagery (Aug. 21, Rev. 795) of the Oklahoma land-cover-classification study area.....30

Figure 3.5 Landsat band-7 image (Oct 11, 1978) of the Oklahoma land-cover-classification study area.....31

Figure 3.6 Standardized probability density distribution of gray level for Seasat descending pass (Aug. 20, Rev. 774) training pixels of the land-cover classification study area.....38

Figure 3.7 Standardized probability density distribution of gray level for Seasat ascending pass (Aug. 21, Rev. 795) training pixels of the land-cover classification study area.....40

Figure 3.8 Standardized probability density distribution of gray level for SIR-A pass (Nov. 13, 1982) training pixels of the land-cover classification study area.....43

Figure 3.9 The effects on the classification accuracy of both Seasat (Aug. 20, Rev. 774) and SIR-A (Nov. 13) data of averaging independent samples (N).....48

Figure 3.10 Summary of multisensor supervised land-cover classification results for the Oklahoma study area. Note that the lower level of each bar is the classification accuracy achieved with a six-pixel, spatially averaged data set.....49

Figure 4.1 Geographic locations corresponding to the Seasat and Landsat images used in the Kansas crop-classification study.....57

Figure 4.2 September 22 Seasat image of the Kansas crop-classification study area.....58

Figure 4.3 October 1 Seasat image of the Kansas crop-classification study area.....59

Figure 4.4 October 7 Seasat image of the Kansas crop-classification study area.....60

Figure 4.5 Landsat band 7 (October 14, 1978) image of the Kansas crop-classification study area.....61

Figure 4.6 Graphical presentation of the means and standard deviations of the crop types for the classification study.....66

Figure 4.7 Generalized crop calendar for the area in Kansas used for the crop-classification study.....67

Figure 5.1 Geographic locations of the five areas used in the selection of forested regions.....84

Figure 5.2 (a) SIR-A image of North Carolina and (b) an example of the mixed forest (M) category. 86

Figure 5.3 (a) SIR-A image of central Kentucky and (b) an example of the deciduous forest (D) category.....87

Figure 5.4 (a) SIR-A image of Alabama and (b) an example of the coniferous forest (C) category.....88

Figure 5.5 (a) SIR-A image of central Brazil and (b) an example of the broadleaf evergreen (E) category.....89

Figure 5.6 (a) SIR-A image of southeastern Brazil and (b) an example of the Galeria forest (G) category.....90

Figure 5.7 Histograms of gray levels for the five forest categories.....93

Figure 5.8 Histograms of contrast for the five forest categories.....94

LIST OF TABLES

		Page
Table 3.1	A Comparison of the System Parameters in the Seasat and SIR-A SAR systems	32
Table 3.2	Category Confusion Table and Separability Measures of the Supervised Maximum-Likelihood Classification for the Seasat (Rev. 774) Pixel Data for the Cultivated (C), Forest (F), Pasture (P), Urban (U), and Water (W) Categories	37
Table 3.3	Category Confusion Table and Separability Measures of the Supervised Maximum Likelihood Classification for the Seasat (Rev. 795) Pixel Data for the Cultivated (C), Forest (F), Pasture (P), Urban (U), and Water (W) Categories	39
Table 3.4	Category Confusion Table and Separability Measures for the SIR-A Supervised Maximum-Likelihood Pixel Classification for the Cultivated (C), Forest (F), Pasture (P), Urban (U), and Water (W) Categories	42
Table 3.5	Category Confusion Table for the Supervised Maximum-Likelihood Classification of the Landsat Data (Bands 5 and 7) for the Cultivated (C), Forest (F), Pasture (P), Urban (U), and Water (W) Categories	45
Table 3.6	Category Confusion Table for the Supervised Maximum-Likelihood Classification of the Combined SIR-A Data and Seasat Ascending and Descending Passes	51
Table 4.1	Category Confusion Tables for the Per-Pixel Classifications and for the Classifications of the Averaged Data for Corn (C), Milo (M), and Wheat (W)	63
Table 4.2	Statistics for the Three Crop Types from All Five Channels Used in the Classification Analysis	65
Table 4.3	Maturity and Harvest Dates for Corn and Milo. Percent of Acreage by Specified Dates for the Southwest Crop Reporting Unit of Kansas (Average of 1973-1977)	69
Table 4.4	Category Confusion Tables for the Multidate SAR Classifications of Corn (C), Milo (M), and Wheat (W)	71

Table 4.5 Category Confusion Tables for the Classification of September 22 Seasat Data with Landsat Band 5 or Band 7 for Corn (C), Milo (M), and Wheat (W).....73

Table 4.6 Category Confusion Tables for the Classification of September 22 and October 1 or October 7 Seasat Data with Landsat Band 5 and Band 7. Categories are Corn (C), Milo (M), and Wheat (W)....75

Table 4.7 Category Confusion Tables for Four- and Five-Channel Multisensor Classifications of Corn (C), Milo (M), and Wheat (W).....76

Table 4.8 Summary of Crop-Classification Studies Using Radar Data... 79

Table 5.1 Description of the Five Forest Types and the SIR-A Data-Take Numbers Used in the Study. All SIR-A Data Were Acquired on November 13, 1981.....85

Table 5.2 Supervised Maximum-Likelihood Classification of Gray Level into the Forest Categories Broadleaf Evergreen (B), Broadleaf Deciduous (D), Mixed (M), Needleleaf Evergreen (E), and Galeria (G).....96

Table 5.3 Supervised Maximum-Likelihood Classification of Contrast into the Forest Categories Broadleaf Evergreen (B), Broadleaf Deciduous (D), Mixed (M), Needleleaf Evergreen (E), and Galeria (G).....96

Table 5.4 Supervised Maximum-Likelihood Classification of Inverse Moment into the Forest Categories Broadleaf Evergreen (B), Broadleaf Deciduous (D), Mixed (M), Needleleaf Evergreen (E), and Galeria (G).....97

Table 5.5 Supervised Maximum-Likelihood Classification of Gray Level and Contrast into the Forest Categories Broadleaf Evergreen (B), Broadleaf Deciduous (D), Mixed (M), Needleleaf Evergreen (E), and Galeria (G).....97

Table 5.6 Supervised Maximum-Likelihood Classification of Gray Level and Inverse Moment into the Forest Categories Broadleaf Evergreen (B), Broadleaf Deciduous (D), Mixed (M), Needleleaf Evergreen (E), and Galeria (G).....99

Table 5.7 Supervised Maximum-Likelihood Classification of Gray Level, Contrast, and Inverse Moment into the Forest Categories Broadleaf Evergreen (B), Broadleaf Deciduous (D), Mixed (M), Needleleaf Evergreen (E), and Galeria (G).....99

CHAPTER 1

INTRODUCTION

1.1 General

Remote sensing, which is the science of acquiring information about an object without physical contact with that object, is being increasingly utilized as a tool in the management of renewable resources. The data produced by remote-sensing systems allow thematic inventories to be produced in a cost-effective and timely manner. In addition, the synoptic perspective provided by satellite systems offers regional coverage unavailable heretofore. For these reasons, remote sensing will become an even more prevalent and important tool for resource management in the coming years.

Remote-sensing systems operate in various parts of the electromagnetic (EM) spectrum, with the visible, infrared (IR), and microwave portions of the spectrum being those most commonly used. Various camera systems, equipped with film sensitive to either the visible or the near-IR wavelengths and deployed aboard aircraft, served as early "sensors" and provided the impetus necessary for the development of more sophisticated sensors. The photography produced by these early remote-sensing systems proved to be very useful for tasks such as crop identification, forest inventory, and geologic mapping. This in turn led to the development of multispectral scanners (MSS), thermal infrared (TIR) systems, and microwave remote sensors. With the launching of the Landsat series of satellites in 1972, the era of space

remote sensing was inaugurated. Today, a wide variety of ground-based, aircraft, and satellite remote-sensing systems operating in the visible, IR, and microwave regions of the EM spectrum provide data for civilian use.

1.2 Microwave Remote Sensing

Microwave remote-sensing systems are relatively new, having been in use only since the early 1960s (Ulaby et al., 1981). Over the last two decades, active microwave systems such as radars and scatterometers, and passive systems such as radiometers, have been developed and tested for various applications. Initially, most imaging radars were deployed aboard aircraft; however, in 1978, Seasat, the first satellite-borne radar, was launched. Unfortunately, Seasat had a fairly short lifetime--only nine months. Since 1979, the only synthetic-aperture radar (SAR) systems to be deployed in space have been those included in the Shuttle Imaging Radar experiments, SIR-A and SIR-B.

Nevertheless, SAR systems continue to be of interest as effective remote sensors and as such are the focus of this investigation. There are several advantages in using radar systems for remote-sensing purposes: one is that they provide their own energy and thus are independent of solar illumination; another is their so-called all-weather capability, which results from the radar's ability to penetrate cloud cover as a result of the long wavelengths employed. This cloud-piercing capability operates independently of weather conditions and thus allows the collection of data during critical time periods. The long

wavelengths used by these sensors also interact with the earth's surface features and thus provide information that is complementary to sensors operating in the visible and IR regions. Moreover, significant penetration into some land-cover types, such as crops and forests, occurs, which provides information about both the vegetation canopy and the soil beneath it.

The sensor parameters of a SAR system--frequency, incidence angle (the angle between the vertical direction and the look direction), and polarization--can also be changed according to the specific application involved. For example, shorter wavelengths and shallower incidence angles, such as X-band (2.4 - 3.8 cm) at 50°, provide information primarily about the plant canopy; whereas longer wavelengths and steeper angles, such as C-band data (3.8 - 7.5 cm) at 10°, provide information about the soil background.

A microwave system can provide data both as a primary sensor and as a backup to conventional MSS systems. In areas characterized by high cloud cover and/or poor solar illumination, such as arctic, coastal, and tropical regions, radar systems can be of great importance because of the difficulty of obtaining optical measurements under such conditions. Although data from microwave systems are not as well understood as optical data, further research and experimentation should make the utilization of microwave data more effective.

1.3 The Multidimensional Approach to Remote Sensing

One of the advantages of using satellite remote-sensing

systems to identify and monitor renewable resources is that such systems have the ability to obtain data repeatedly throughout the year. It has long been recognized that multitemporal data can reduce ambiguities in the interpretation of remotely sensed data (Goodman, 1959). This is especially true in land-cover mapping, as a result of the dynamic temporal patterns of the earth's surface features. For example, when using optical systems, corn and soybeans may be indistinguishable from each other early in the growing season; however, they may become identifiable later, as the corn ripens and develops its characteristic golden color.

It is also possible to increase the specific information content of radar data by using different system configurations. Three fundamental system parameters--frequency, incidence angle, and polarization--can be varied to obtain data from different surface features. Ulaby (1982) provides an overview of the radar signatures of terrain and discusses the influence of varying system parameters on the radar energy backscattered by different terrain elements.

Another approach to increasing the information content available for a particular task is to use sensors designed to respond to different portions of the EM spectrum. For example, multisensor approaches have been investigated both for crop-classification purposes (Ahern et al., 1978; Ulaby et al., 1982) and for land-cover classification (Wu, 1980), and it has been shown that classification accuracies tend to increase when multisensor data are used. This is because two surface features may be confused in the microwave region but separable in the

optical region--for example, forest cover and urban areas, which are separable optically but may be confused with each other when microwave data are used.

In most remote-sensing applications, image tone is the feature most commonly used for image interpretation. Image texture, the spatial distribution of the image tone in a target area of interest, is also a useful feature and can be of considerable value in the analysis of radar data (Berger, 1970; Lowry et al., 1978; Shanmugan et al., 1981a). Although digital classifications based on image texture are not now readily available, they promise to increase both information content and classification accuracy. Haralick (1979) provides a review of both the statistical and the structural approaches to image texture.

Multidimensional data sets offer great potential for various remote-sensing applications. Furthermore, the dimensions can be increased by acquiring multitemporal data, varying the sensor parameters, using sensors designed to respond to different portions of the EM spectrum, and using a combination of image tone and texture.

1.4 Scope of the Investigation

This study focuses on the use of satellite SAR data for mapping land-cover types. The investigation comprises three tasks. In the first, land cover in Oklahoma is mapped at the primary level (see Anderson et al., 1976), using image tone to interpret Seasat, SIR-A, and Landsat data. The second task

involves the classification of crop types in western Kansas using image tone from multitemporal Seasat data augmented with one date of Landsat data. In the third task, image tone and texture in SIR-A data for forest types from five different forest biomes are analyzed to determine the suitability of satellite SAR data for mapping forest types. The three studies are reported in Chapters 3, 4, and 5, following a general literature review in Chapter 2. The results of the studies are then used to assess the use of satellite SAR data for land-cover classification purposes and the relative merits of the different multidimensional approaches.

There has been a paucity of research concerning the use of satellite SAR data, partly because data are not generally available and partly because of the nature of the data that are available. For example, the satellite SAR systems that have been launched to date have been designed for applications other than mapping and monitoring renewable resources. As a result, the approach used in this investigation is one of empirical observation and subsequent explanation, rather than of theoretical model development and testing. The results of these three studies will allow the development of working hypotheses on land-cover mapping using satellite SAR data, both alone and in combination with satellite MSS data. The scene will then be set for the initiation of further research into and development of operational models. This will in turn bring the use of SAR data closer to the operational level and thereby increase the number of applications to which remote sensing can be applied.

CHAPTER 2

BACKGROUND INFORMATION AND LITERATURE REVIEW

2.1 Introduction

Since the mid-1960s, imaging radar systems have been providing imagery for a variety of natural-resource, land-use, and environmental studies (Estes and Simonett, 1975). Although plan-position-indicator (PPI) and B-scan airborne radars have been available since the middle of World War II, it is the side-looking airborne radar (SLAR) systems that are used for these types of investigations today (Moore, 1975). The PPI and B-scan radars produce displays that are essentially binary in intensity by representing the presence or absence of objects responsible for the backscattering of microwave energy. Imaging radars, on the other hand, measure the strength of the backscattered signal and therefore provide more information than the original PPI and B-scan radars. Furthermore, the techniques required to interpret the imagery from these new radars is different from the PPI and B-scan systems, so experimentation is needed to determine how these types of data can be most effectively used. As Moore (1978) points out, microwave systems of various types have been used in a wide variety of land and ocean applications.

Before the operational use of radar data becomes a reality, appropriate methodology must be developed. Two basic approaches have been used to develop methodology and to obtain a better understanding of microwave interactions with the earth's surface features. One approach involves the collection of imagery from

aircraft and spacecraft and the subsequent interpretation of the data acquired for the target(s) of interest. In this approach, image tone and texture are the key elements of interpretation. Another approach makes use of ground-based radar systems that provide point radar backscattering (σ^o) measurements that are subsequently analyzed using both statistical and graphical techniques. Bradley and Ulaby (1980) have shown correlations ranging from .8 to .92 in a comparison of ground-based versus airborne σ^o measurements.

This chapter presents an overview of radar remote sensing as it is used for mapping and monitoring land use, forestry, and agriculture. Emphasis will be placed on results reported in the literature, based on radar imagery, for these applications. A brief introduction to radar-image interpretation will be included, and the differences between visible/infrared techniques and radar methods noted. Significant ground-based studies will be included where appropriate.

2.2 Interpretation of Radar Imagery

Side-looking radars produce a continuous image strip that resembles a grainy aerial photograph taken from a great altitude (Estes and Simonett, 1975). However, the microwave region of the EM spectrum responds to different target and system parameters than do the other regions. Estes and Simonett (1975) suggest that the following factors influence the appearance and interpretability of radar images: (1) system geometry, including flight parameters, (2) resolution in ground range, (3) resolution

in azimuth, (4) areal resolution, (5) number of independent samples, and (6) backscattering cross section per unit solid angle directed toward the radar receiver. The last factor determines the brightness of any given resolution cell and is a function of the dielectric and geometric properties of the target being imaged (Ulaby, 1975). The backscattering governs the tone of the image, and the spatial distribution of the tone in any given field of interest represents image texture.

As with visible and infrared images, tone is a key element in image interpretation. Nonetheless, texture is a useful discriminant in the interpretation of radar imagery as well (Berger, 1970; Lowry et al., 1978; Shanmugam et al., 1981a). Other elements of image interpretation described by Estes and Simonett (1975), such as shape, size, and location, are also useful in the interpretation of radar imagery. Thus, the elements of image interpretation and the techniques utilized in radar-image analysis are similar to those used in the interpretation of visible and IR data, with differences in system parameters and target interactions taken into consideration. Moreover, different emphases are placed on the interpretation of tone and texture during the analysis of radar imagery; for example, texture is used to discriminate targets imaged with microwaves, whereas tone is used to analyze MSS and visible data.

Some examples of image-interpretation techniques that have been applied to radar imagery follow. Ellermeier et al. (1967) describe the use of color enhancement and level slicing for both agricultural and natural vegetation discrimination. In their

study, electrical analogs of the scanned images were fed into three (red, blue, and green) electron guns and displayed on the cathode-ray tube of a color television set. Various combinations of images in varying colors could then be reproduced to aid in image interpretation. Coiner (1972) proposes the use of image-interpretation keys to support the analysis of SLAR imagery. For example, a dichotomous key using image tone and texture was developed to discriminate crop types appearing on images of Garden City, Kansas. A similar approach was used by Brisco and Protz (1980) to identify corn fields using multidate, multichannel, radar data. The results of both studies indicate that this approach is feasible for radar-image interpretation. Larson et al. (1975) present the use of multichannel analysis techniques familiar in multispectral scanner (MSS) data analyses. These techniques include image ratioing, subtraction, level slicing, maximum-likelihood classification, and Euclidean distance-clustering. Their results were promising and indicated that these techniques can be applied to microwave data.

In the preceding examples, digital-analysis techniques employed tone, for the most part, as the element of discrimination. The use of texture was incorporated into manual interpretations using dichotomous keys and a subjective evaluation of texture (i.e., smooth, medium, or rough texture). The value of texture as an element in the interpretation of radar imagery has long been recognized (Berger, 1970; Coiner, 1972; Lowry et al., 1978). Ulaby et al. (1982) compared within-field and between-field coefficients of variation for several cover types, using

Landsat images and Ku-band scatterometer data. They concluded that the radar data exhibit larger within-field and between-field variations than the Landsat data. Thus, improvements in machine classification can be expected as techniques are developed to incorporate a digital measure of texture into the discrimination procedure (Shanmugam et al., 1981; Brisco and Protz, 1982).

Since it was found that classification techniques similar to those being applied to various forms of MSS data could be applied to radar data, research was initiated into combining these types of data for analysis. Harris and Graham (1976) present images formed from a combination of Landsat and radar data. Zobrist et al. (1979) present integrated Landsat, Seasat and other geodata sources, thus illustrating that the technique can be used for virtually any digital data which can be registered to a common spatial framework. In the following sections, radar remote sensing for land-use, forestry, and agricultural work will be presented, with the aim of illustrating the advantages of the techique.

2.3 Land-Cover Mapping with Radar

With the increasing demands being placed on natural resources by a rapidly expanding population and the concomitant necessity of maintaining environmental quality, there is a need for an orderly grouping of various areas of the earth's surface (Gimbarzousky, 1978). Land-use and land-cover maps have become ever more important as a source for such information. Anderson et al. (1976) provide a framework for a national land-use and land-cover

classification system for use with remote sensor data.

Some early studies showed that accurate land-use/land-cover classification at different levels can be achieved using radar imagery (Lewis, 1968; Lewis et al., 1969; and Bryan, 1975). Drake (1977) pointed out, however, that the United States Geological Survey (USGS) system presented by Anderson et al. (1976) must be adapted before it will accept radar data readily. They suggest that there is a lack of compatibility between the system and the data because of the nature of radar imagery compared to that of the optical imagery for which the classification system was developed. As a result, Drake (1977) presents an alternate classification system for use with radar imagery.

Henderson (1975) used Westinghouse K-band radar imagery for small-scale (1:250,000 or smaller) land-use mapping and found that the majority of the land-use regions identified on the basis of the imagery corresponded to land-use regions established by other methods. Where differences occurred, finer distinctions in land-use were apparently generated from the radar image interpretation. This study further indicated that radar imagery is a useful tool in small-scale land-use mapping but suggested that additional testing is needed to verify the utility of the method. In another study using similar data, Henderson (1979) reported that land use in the northeastern and midwestern United States was identifiable at Level I detail without much difficulty. He concluded that the paramount factor affecting detectability and identification was the presence of forest vegetation. Trees and forest canopy concealed drainage features,

topographic variations, transportation arteries, etc., which hindered land-use classification. The problem of concealment was greater in the Northeast than the Midwest because of the larger field patterns and more homogeneous land use and cover types found in these regions.

Airborne SAR imagery obtained over two test areas in southwestern Manitoba (Canada) was used successfully for land-use/land-cover mapping by Rubec and Cihlar (1980). They employed a four-channel SAR system developed by the Environmental Research Institute of Michigan to collect imagery and found that the most extensive information appeared on the X-band images. However, they suggested that a combination of X- and L-band data be used for maximum interpretation success. Using imagery collected by the same system over Halifax County and comparing it with other remote-sensing data including Seasat SAR, Prout (1980) found that the ERIM SAR data could be used for mapping urban areas, improved pasture and crops, water, and transportation. Prout reported that the Seasat SAR data could not readily classify any of these land-use/land-cover categories. The results of the Landsat interpretation were slightly better than those of the Seasat SAR, whereas the best results were obtained using conventional aerial photography. Prout (1980) concluded that each remotely sensed data source contributed some information toward the mapping of land-use categories, and when used in various combinations, the information was complementary and reduced the time necessary for the detection and identification of land-use features.

Henderson et al. (1980) investigated the detectability of urban land-cover types using digitally processed Seasat SAR imagery of the Denver, Colorado area. They employed and compared both traditional manual-interpretation techniques (utilizing image tone and texture as well as other elements of interpretation) and digital level-slicing using the Image 100 computer to determine the separability of urban-area land-cover types. In general, level-slicing and color coding the raw data tended to reduce both the level and type of information available when compared to visual observation. However, the extent of urban, built-up land was more easily detected using this method. In conclusion, they reported a readily definable rural-urban fringe; however, a precise Level I or Level II land-cover classification was not possible. High-density housing was separable from both low-density housing and parks, but reflectance values were often look-angle dependent, and confusion between water and vegetation responses also posed problems. Nevertheless, the authors concluded that continued research into reducing image noise and choosing an optimal scale for recognizing land-use patterns may improve the utility of a spaceborne-SAR system for use in urban analysis.

Another area of research that promises to improve the utility of satellite radar systems for land-cover mapping is the merging of microwave data with MSS data. Wu (1980) registered Seasat SAR with Landsat MSS data and used conventional multichannel spectral pattern-recognition techniques for land-cover classification. He reported further subdivision in the classification of forested

wetlands and improvement in discriminating man-made targets (i.e., urban and inert classes) with the combined data, when compared to Landsat data alone.

2.4 Forest-Cover Mapping with Radar

Forest reserves worldwide are rapidly diminishing as an expanding population increases its demand for wood products to be used in building and heating. Simultaneously, forests are continually being cleared to increase agricultural productivity and to provide living space. As a result, with the launch of Landsat, the first remote-sensing satellite, in July 1972, many researchers began studying the potential of remotely sensed data for use in forest inventorying (Beaubien, 1978). The results were promising, and remote-sensing techniques have now been implemented in the mapping and management of the forest resources in Canada (Honer, 1978).

Morain and Simonett (1966), in an early study of vegetation analysis using radar imagery, concluded that the influence of vegetation upon radar returns was observable in all of the areas of the United States that were investigated. By using tonal and textural comparisons of K-band imagery combined with basic geographic knowledge of the study area, it was possible to (1) prepare reconnaissance vegetation maps, (2) delimit vegetation zones as they vary with elevation, (3) trace patterns of previous forest fires, (4) delimit altitudinal timber lines, and (5) identify species by inference in areas characterized by near-monospecific stands. In a follow-up study, Morain and Simonett

(1967) used electronic techniques to discriminate patterns of vegetation distribution. The techniques included the use of tri-color image combinations, the generation of probability-density functions to quantify variations in gray-scale level between types, and the employment of density slices to help distinguish among vegetation types. These methods were found effective in the discrimination of pine, fir, hardwood forests, and juniper woodlands because subtle differences indistinguishable to the unaided eye were brought to the attention of the interpreter. The studies demonstrated the potential of SLAR imagery for forest-cover mapping.

One of the first and most ambitious uses of SLAR for forest mapping was undertaken in Brazil by the Goodyear Corporation, using a K-band SAR system (Azevedo, 1971). Project RADAM (RADar AMazon) produced geologic, geomorphologic, hydrologic, vegetation-cover, soil-type, and land-use-potential maps of the Amazon River Basin. Because the high incidence of cloud cover in the region, as well as its remoteness, made aerial photography difficult, radar imagery helped to produce some of the first vegetation-cover maps of the region. Viksne et al. (1970) point out that because K-band radar does not penetrate the forest canopy, it allows the evaluation of various vegetation types on the basis of their radar-return characteristics. These authors described the use of K-band SLAR for vegetation mapping in Panama, a project similar to the RADAM project.

Waite and MacDonald (1971) suggest that the insignificant penetration into vegetation at K-band allows interpretations of

variations in the density of plant communities to be made. However, they also report that for defoliated vegetation, the K-band frequency may penetrate a forest canopy significantly and thus allow differences in underlying soil moisture to be observed. They also report using the depolarized return signal to differentiate both gross vegetation differences and soil-moisture variations. Bush et al. (1976) describe ground-based, 1 - 18-GHz microwave observations of deciduous trees during the spring and autumn. The data suggest that trees act as a volume-scattering target and that σ^0 is substantially larger in the spring than in the fall. These results further indicate that penetration varies seasonally and thus must be taken into consideration when performing interpretations of vegetative cover.

Morain (1976) presents three levels of vegetation information obtainable from the analysis of radar data: (1) geographic pattern, (2) gross structure and physiognomy, and (3) type identification. Interpretation relies on converging evidence derived from principles of geography, biology, and ecology, combined with the interpreter's understanding of radar reflection from vegetation. Using such an approach, Hardy (1972) was able to produce a seven-category vegetation map of Yellowstone Park using the Westinghouse AN/APQ-97 SLAR system. Both authors report that tone and texture are key elements in radar-image interpretation, but that continued development of methodology is required before the operational use of radar for vegetation mapping is feasible.

Intera (1980), in a presentation of the final results of the Airborne SAR Project (a component of the Canadian SURSAT program),

presents the experiments of several investigators researching the utility of radar for monitoring and mapping forests. These studies indicate that radar may be used either alone, on some occasions, or to provide ancillary data to MSS sensors monitoring aspects of the forest environment such as regeneration, insect infestation, and environmental disturbances resulting from human activity; interpreting broad age and height classes; and providing input to the production of vegetation-type maps. The studies used the ERIM dual-polarized SAR system and, in general, concluded that tone and texture for both the like- and cross-polarized images of the X-band and L-band frequencies provided information about the forest environment. Knowlton and Hoffer (1980) also investigated the use of the ERIM SAR system for forest-cover mapping. They qualitatively evaluated the tone and texture of the dual-polarized X-band images for their value in identifying various forest-cover types. The results showed a greater tonal contrast overall on the HH image than on the HV image but also showed that both channels provided information on certain forest-cover features. These authors qualitatively evaluated image texture in their study but did not report any uses of this image-interpretation element in their conclusions. Knowlton and Hoffer (1980) suggest future research investigating spatial pattern recognition (ECHO) using these data to classify forest and other cover types, since some differences in image texture were observed.

It has been demonstrated that SAR data can provide valuable input for monitoring and mapping the forest environment. Texture is a key element, and the digital analysis of this image

characteristic must be developed before automatic classifications of high quality will be possible. This development, coupled with a better procedure for registering other data sets--for example MSS and topographical data--may well result in the operational use of radar for forest reconnaisance.

2.5 Agricultural Discrimination with Radar

The monitoring and mapping of agricultural land is perhaps even more critical than the inventorying of land use and forest cover, since man relies heavily on agricultural production to form his food base. The need for improved world crop statistics and for the development of an information system capable of providing such data is reviewed by King (1979). Remote-sensing techniques can provide timely and valuable data for such a system, as Bauer (1975) points out. Although accurate crop identification using multitemporal MSS data is becoming an established procedure (Lacie Symposium, 1978) a problem with interrupted coverage due to weather conditions exists. Radar may help solve this problem because of its all-weather capability and because of the active nature of its operation (Ulaby, 1981). Although agricultural discrimination involves both soil-moisture and crop-type implications, this discussion will focus on the latter. Batlivala and Ulaby (1976b) and Ulaby et al. (1981b) provide excellent accounts of monitoring soil moisture with radar. The results of these studies indicate that a C-band dual-polarized radar using incidence angles in the neighborhood of 10 degrees provides the best data for estimating soil-moisture conditions.

Early research investigating the crop-identification ability of radar demonstrated that crop type largely influences radar return; thus, discrimination is possible (Simonett et al., 1967; Schwarz and Caspall, 1968; and Haralick et al., 1970). These differences were attributed to variations in plant geometry and moisture content between crop types, which subsequently caused different tonal and textural patterns on the K-band imagery. Analysis techniques included manual-interpretation keys, the digital classification of tone, color enhancement, and density slicing. The results were promising and led to continued research into the use of radar for crop discrimination.

The radar return from a given target is a function of both system and target parameters and their interaction. In general, the system parameters of importance are frequency, incidence angle, and polarization, whereas geometric and dielectric characteristics are the most important target parameters. These parameters and their relationship with σ^o are discussed in some detail by Ulaby and Moore (1973) and Ulaby (1975). Cihlar (1979) provides a review of active microwave remote sensing of agricultural targets and describes significant research results relating to the investigation of target and system parameters, their interaction and their effects on σ^o.

As a result of the promising results of the early studies, a well-developed research program has been established at the University of Kansas to investigate the crop discriminating ability of radar. Ground-based radar systems have been developed and employed for these studies because of the paucity of

calibrated airborne radars (Ulaby, 1981). Bradley and Ulaby (1980) have demonstrated high correlations with airborne and ground-based data, which allows the use of the results obtained from truck-mounted Microwave Active Spectrometer (MAS) systems in interpreting airborne radar data.

These studies have investigated the relationship of σ^o, which represents image tone, to various system and target parameters. The results have helped both to identify and to increase our understanding of the relationships between σ^o and crop type (Ulaby, 1975), row-direction effects (Batlivala and Ulaby, 1976b; Ulaby and Bare, 1979), plant moisture (Ulaby and Bush, 1975, 1976), growth stage (Bush and Ulaby, 1975), and diurnal fluctuations (Ulaby and Batlivala, 1976). Using the relationships established by these investigations, the feasibility of using radar data for crop classification were evaluated (Bush and Ulaby, 1977a, 1977b; Ulaby and Burns, 1977). The results were also used to identify operational system parameters for a future spaceborne radar system (Bush and Ulaby, 1977c; Ulaby et al., 1977). A later study demonstrated that a year-to-year consistency in crop classification of approximately 90% correct prediction could be achieved with ground-based σ^o values (Ulaby et al., 1979). Studies conducted by European investigators have also substantiated these findings (de Loor and Jurriens, 1971, 1974).

As mentioned above, comparatively few studies have been conducted using airborne platforms. Batlivala and Ulaby (1975) investigated the use of L-band dual-polarized radar imagery for crop discrimination. They reported a 65.5% correct classification

with L-HH data for corn, soybeans, woods, and pasture using image tone. When the L-HV data was used with the HH data, classification accuracy rose to 74%. Brisco and Protz (1980) reported corn classification accuracies exceeding 90% using the ERIM four-channel radar system but an overall accuracy of only about 50% for hay-pasture and grain fields (Brisco and Protz, 1982). Parashar et al. (1979) also used the ERIM system to investigate the radar discrimination of crops. They reported that the multichannel data provided more information for crop discrimination than either channel alone. They could readily detect differences between harvested and unharvested crops but found a high degree of confusion among the numerous crop types considered. Both Brisco and Protz (1980, 1982) and Parashar et al. (1979) used image tone and texture in their manual interpretations. Image texture could not be readily used in the digital analysis, which resulted in comparably poorer classifications using automatic techniques. Shanmugam et al. (1983) investigated the use of airborne multidate/multifrequency radar data over a test site near Colby, Kansas. They reported an overall accuracy of about 90% for corn, pasture, and bare ground using C- and L-band multidate scatterometer data, with σ^0 values representing tone.

The results of these investigations are encouraging and demonstrate the potential of radar as a crop classifier. The use of multidate radar data, combined with MSS data, promises even better results in the future (Ahern et al., 1978; Eyton et al., 1979; Ulaby et al., 1982). Although the methodology for the

operational use of radar data in a crop-information system is as yet not established (King, 1979), future research and development should produce the necessary techniques. Texture has been used extensively in the past for visual radar interpretations, and the methodology for automatic extraction of spatial information is being developed. This, combined with multitemporal, multisensor data, should allow the operational use of radar for crop discrimination in the future.

2.6 Summary

Since the mid-1960s, radar systems have been providing imagery of a variety of natural-resource, land-use and environmental studies. These systems offer several advantages over alternate remote-sensing systems, but methodology needs to be developed before their operational use will become feasible. This chapter summarized the use of radar for the remote sensing of land-use, forest, and agricultural targets. Research papers were surveyed and the results of the major investigations in these areas of study were presented. In each case, the results showed that the use of radar for these applications is feasible. However, the studies uniformly point out that suitable methodology must be developed before the operational use of radar is possible. Two areas of research that appear promising for the improved use of radar were discussed. It was found that the use of integrated data sets and digital measures of image texture have resulted in improvements in land-use mapping and crop discrimination.

Image texture is a valuable component of radar image analysis, and the development of an automatic textural measure for machine classification is expected to greatly improve the utility of radar data for agricultural, forestry, and land-use mapping. The combination of microwave data with data from other sensors such as MSS, and with other geodata such as soil information, also promises to improve greatly the utility of radar for classification and mapping, as more information is provided by these complementary data sources. The continued development of radar remote-sensing techniques can be expected to produce an operational methodology for use with these types of data when geoscientific investigations are undertaken.

CHAPTER 3

LAND-COVER MAPPING IN OKLAHOMA

3.1 Introduction

At the time of this study, only two spaceborne microwave systems, Seasat in 1978 and the Shuttle Imaging Radar-A (SIR-A) in 1981, had provided radar imagery of the earth's surface (Jordan, 1980; Elachi, 1982). Whereas Seasat's main operational thrust was toward oceanographic applications, studies utilizing SIR-A data have concentrated on geology. As a result, comparatively little research has been conducted on the utility of spaceborne synthetic-aperture radar (SAR) data for monitoring and inventorying the earth's renewable resources. Nevertheless, the imagery these two space-SAR systems have produced demonstrates clearly the feasibility of (1) generating high-resolution radar imagery using a satellite platform as a base and (2) extracting useful information from radar images for use in terrain applications.

This study investigates the use of spaceborne SAR data for land-cover mapping. The land-cover classification accuracy achievable with Seasat data was compared with that obtainable using SIR-A data and Landsat MSS data. A supervised maximum-likelihood classifier was used in the analyses on both a per-pixel basis and on spatially averaged data. The image data were then merged in several multichannel combinations and reclassified in order to determine the optimum combined-image data set for land-cover classification.

3.2 Image Data and Test-Site Description

In August of 1978, the Seasat satellite imaged an area in Oklahoma on both the descending (August 20, Rev. 774) and ascending (August 21, Rev. 795) orbits. On November 13, 1981, the SIR-A system acquired SAR imagery of Oklahoma (Data-Take 22, Orbit 18). A portion of the imaged area was identical to the area imaged previously by the Seasat satellite. The nominal scale of the SAR data sets was 1:500,000, with a resolution of 25 m for the Seasat data and 38 m for the SIR-A data. On the same day, an aircraft flying at a low altitude obtained color and color-infrared (CIR) photography (scale ≈ 1:20,000) of a portion of the area imaged by the SIR-A radar for ground-truth purposes. A Landsat scene from October 11, 1978 (Scene ID No. 30220-16242) also covered this area of Oklahoma. The overlapping regions of the data sets determined the location of the study area (Figure 3.1). Examples of these SAR images and band 7 of the Landsat scene are presented in Figures 3.2 - 3.5. The Seasat and Landsat images were initially acquired in digital form, whereas a portion of the SIR-A imagery, corresponding to the study area, was digitized at Goddard Space Flight Center (GSFC). A digitizing aperture of 100 μm was used, which approximated the original pixel size of the SIR-A data such that no spatial averaging occurred in the digitization process. A comparison of the system parameters for the Seasat and SIR-A sensors is presented in Table 3.1.

Cover types for the classification analyses were selected on the basis of color-infrared photography and a field visit. Five land-cover types were chosen, consisting of cultivated (hay,

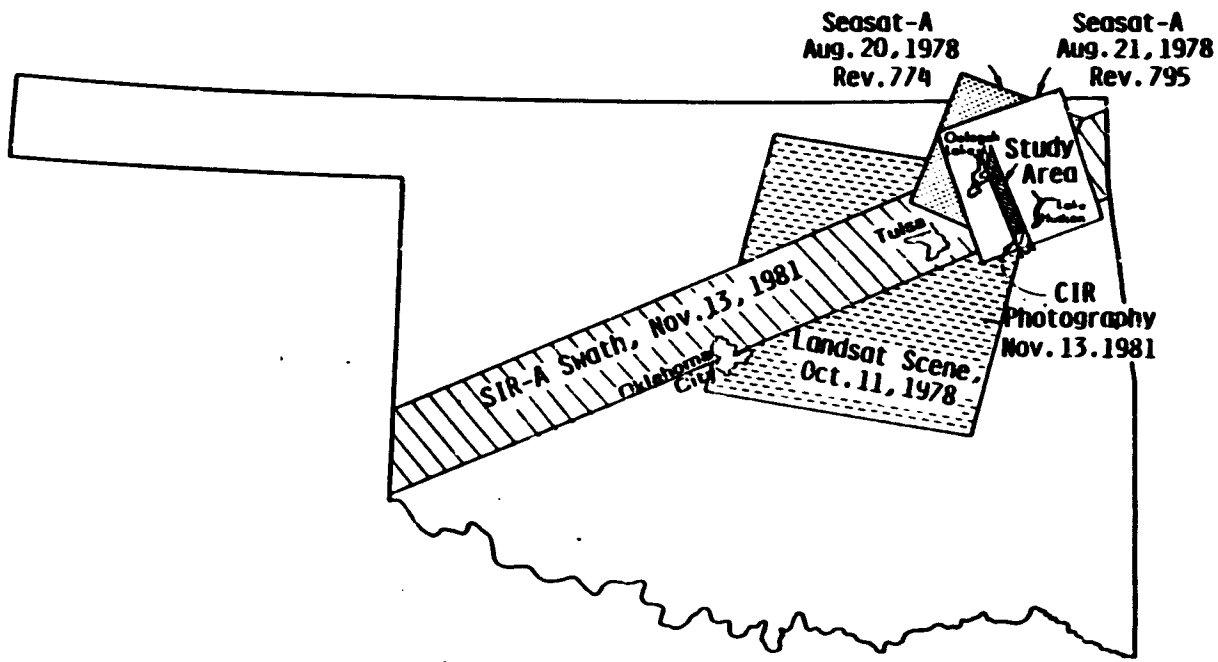

Fig. 3.1. Geographic locations corresponding to the SAR and Landsat images of Oklahoma, with the land-cover classification study area delineated.

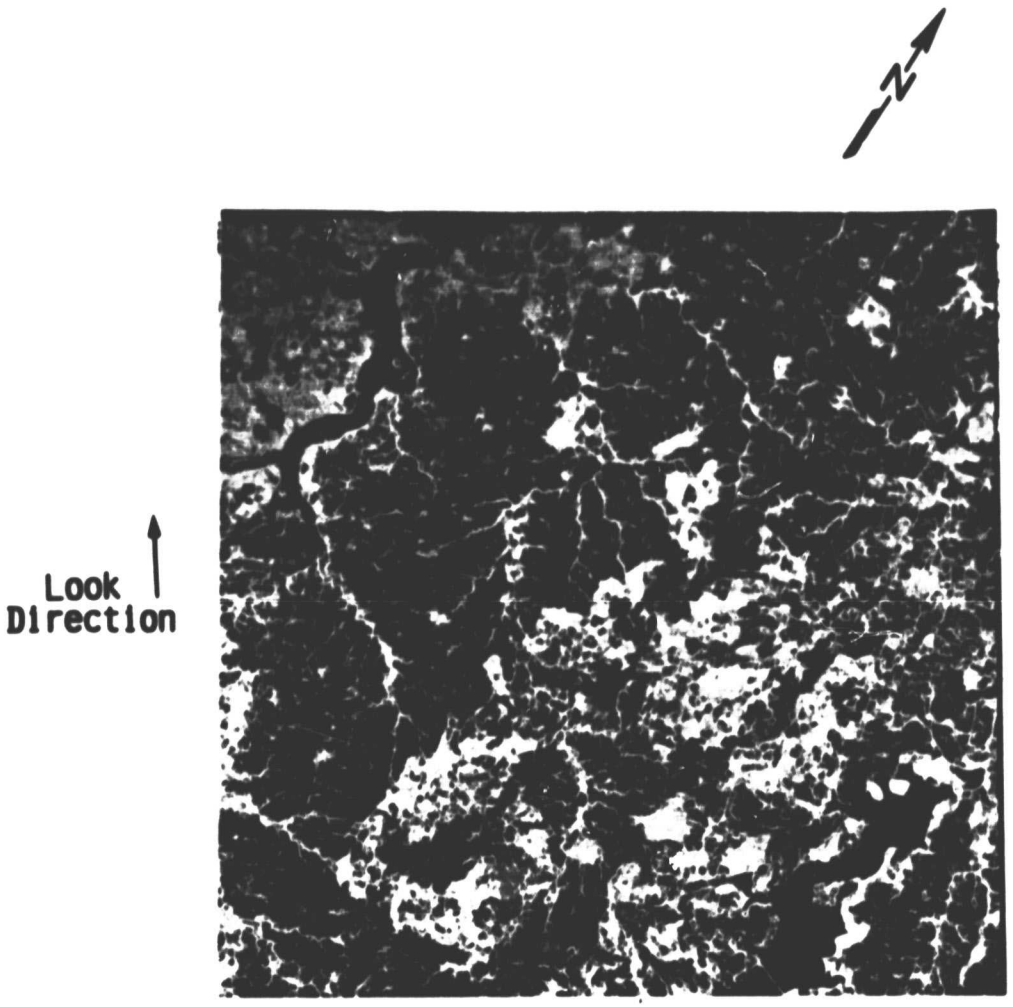

Fig. 3.2. SIR-A imagery (Nov. 13, 1982) of the Oklahoma land-cover classification study area.

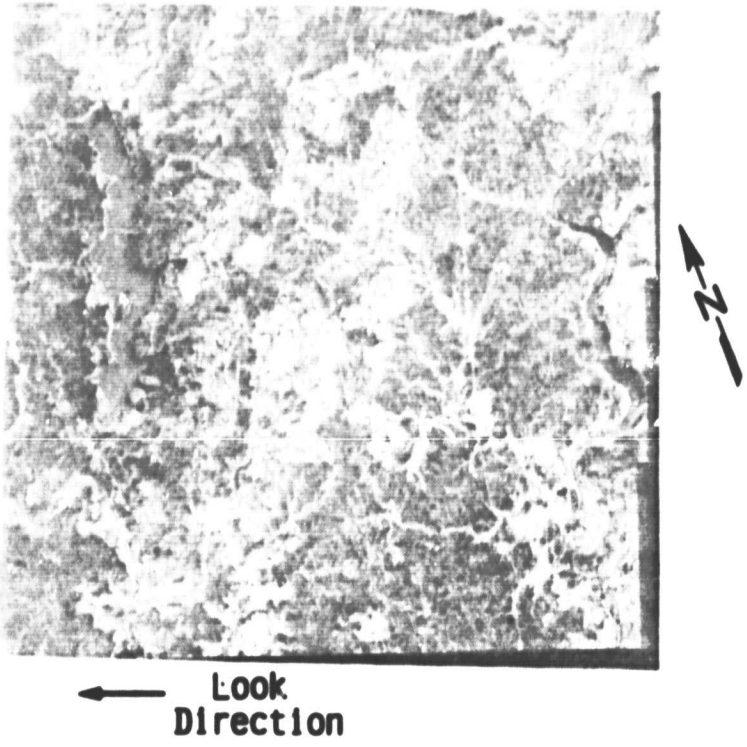

Fig. 3.3. Seasat imagery (Aug. 20, Rev. 774) of the Oklahoma land-cover classification study area.

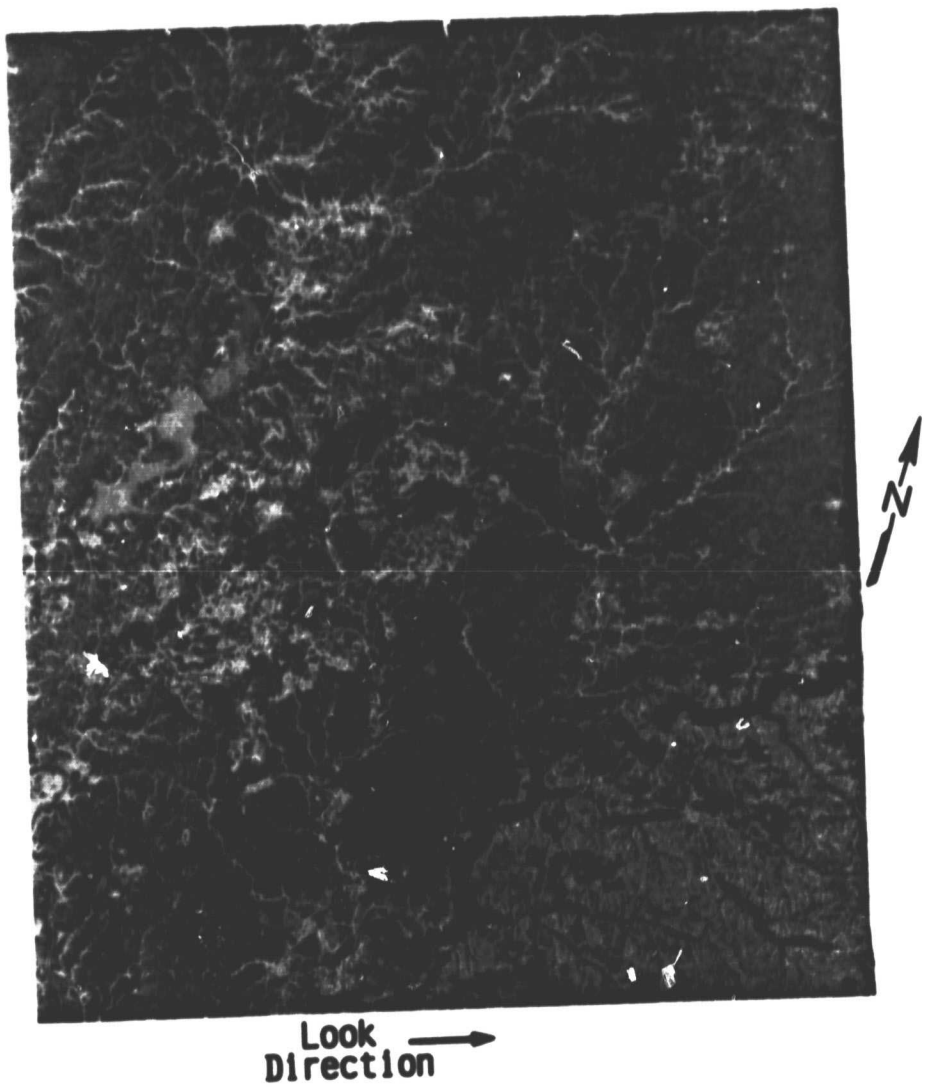

Fig. 3.4. Seasat imagery (Aug. 21, Rev. 795) of the Oklahoma land-cover-classification study area.

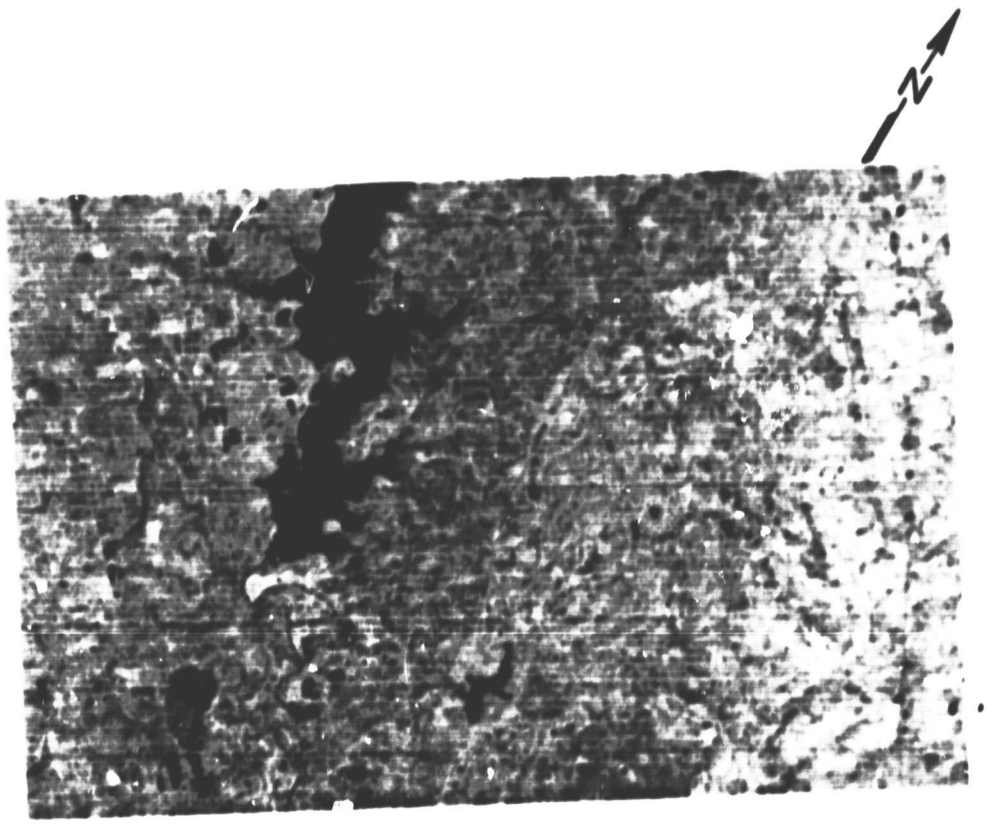

Fig. 3.5. Landsat band 7 image (Oct. 11, 1978) of the Oklahoma land-cover classification study area.

TABLE 3.1

A Comparison of System Parameters in the Seasat and SIR-A Synthetic-Aperture Radar Systems

Parameters	Seasat	SIR-A
Frequency	1.275 GHz	1.278 GHz
Incidence Angle	20°	50°
Polarization	HH	HH
Resolution	25 m	38 m
Number of Looks	4	6
Swathwidth	100 km	50 km
Orbital Altitude	800 km	245 km

winter wheat, and bare soil), forest, pasture, urban, and water categories. An attempt was made to locate ten fields, representing each land-cover category to be used for the supervised classification, by inspecting the CIR photography. A subsequent check was made to ensure that these fields could be identified on the satellite imagery. However, within the study area, there were only five cultivated fields sufficiently large to allow data extraction, and only one body of water (Oologah Lake), which was sampled at five locations. Thus, 40 fields, ten each of the urban, forest, and pasture categories and five fields of the water and cultivated categories, were used in the study. The ten fields representing the urban category were from the towns of Chelsea, Chouteau, and Pryor, Oklahoma. Due to the smaller scale of the Landsat data, some of the fields could not be delineated. Thus, although 40 fields were used in the SAR analyses, only 32 were actually identified on the Landsat imagery.

3.3 Methodology

The corner-point coordinates for each of the 40 fields, taken from inside the field's boundaries, were determined for each image data set on the University of Kansas Remote Sensing Laboratory's (RSL) image-analysis system. These data were then extracted, using RSL's Harris 230 computer facility, for subsequent maximum-likelihood supervised classification analyses. There were at least 10,000 pixels in each SAR data set. Maximum likelihood, or Bayes' optimal classification is an intuitively satisfying classification theory because it minimizes overall

misclassification. Swain and Davis (1978) provide an excellent description of maximum-likelihood classification theory.

Per-Pixel Classifications

For each SAR data set, a 10% random sample of the pixels in each category was used to train the maximum-likelihood classifier. These training statistics were then applied to the remaining 90% of the pixels. Category-confusion tables and a common measure of category separability known as the Normalized Difference (ND), defined as the difference in the category means divided by the sum of their standard deviations, were generated for each classification performed. The pixels in each category were then plotted as normalized probability density distributions. These three results (hereafter called classification attributes) were then used to evaluate and compare the overall weighted classification accuracies obtained for each supervised classification. For the Landsat MSS data, bands 5 and 7 were used simultaneously for the per-pixel classification of the 32 identifiable fields.

Spatial Averaging

Fading, represented by image speckle, is inherent in SAR data as a result of the coherent nature of the propagated signal (Bush and Ulaby, 1975). The effects of fading can be reduced by averaging the number of independent observations, either in the frequency domain or in the spatial domain. To investigate the influence of fading on land-cover classification accuracy, the

resolution of the SIR-A and Seasat (descending orbit) data was degraded by averaging blocks of pixels in a stepwise manner, i.e., 2 x 2 pixels, 3 x 2, 3 x 3, etc., and the spatially averaged data then reclassified.

Per-Field Classifications

All image data sets (including Landsat) were then averaged with a 6-pixel by 6-pixel filter, and the resulting data were used in a per-field supervised classification. Note that each field in this case is actually a 6- x 6-pixel subfield formed by averaging as many 6- x 6-pixel blocks from the original fields as possible. This procedure produced at least 100 "fields" for each SAR data set. In all of the classification analyses of spatially averaged data, a 50%-training, 50%-testing sample was employed.

Various multichannel/multisensor combinations were then combined and classified using a 50%-training, 50%-testing sample. However, this was done on a whole-field basis (rather than the 6- x 6-pixel "fields" described above), since there was no attempt to register the image data sets on a pixel basis because of differences in the resolutions and geometries of the various sensors. The interpretation of the influence of spatial averaging and multichannel combinations on land-cover classification accuracy was based on a category-confusion table.

3.4 Pixel Classifications

The weighted overall classification accuracy obtained for the testing sample of the Seasat (descending pass, Rev. 774) pixel

data was 49.86%. Table 3.2 presents the category-confusion table and separability measures for the supervised classification. Pasture was the most accurately identified category (77%), followed by the forest, water, urban, and cultivated categories. The forest and urban pixels produced the brightest tones on the image, whereas the pasture, water, and cultivated categories all had low tonal values. The standardized probability density distribution (Figure 3.6) illustrates the range of pixel values for these categories on the descending Seasat image.

As the classification attributes presented in Figure 3.6 and Table 3.2 indicate, the pixels in any given category have a large standard deviation and a low separability, resulting in the poor classification accuracy of approximately 50%. The pasture category, with a relatively small standard deviation (6.63) and dark tonal levels, is the most accurately classified category. Urban pixels are highly confused with forest pixels and to a lesser extent with water and pasture pixels. Water pixels are largely misclassified as pasture pixels and secondarily as forest pixels. The cultivated pixels are never accurately classified, since their range of tonal values is completely enveloped by the pasture and water pixels.

The weighted overall classification accuracy obtained for the ascending Seasat pass (Rev. 795) was 50.32%. This is very similar to the results for the descending Seasat pass, although differences in category confusion related to orthogonal look direction are present (Table 3.3, Figure 3.7). The tonal values of the water pixels were brighter on the ascending pass as

TABLE 3.2

Category Confusion Table and Separability Measures of the Supervised Maximum-Likelihood Classification for Seasat (Rev. 774) Pixel Data for the Categories Cultivated (C), Forest (F), Pasture (P), Urban (U), and Water (W)

	Category				
	C	F	P	U	W
Mean	19.44	34.89	17.70	48.81	20.37
Std. Dev.	6.81	13.04	6.63	29.67	6.92

Separability

C-F	C-P	C-U	C-W	F-P	F-U	F-W	P-U	P-W	U-W
0.78	0.13	0.81	0.07	0.87	0.33	0.73	0.86	0.20	0.78

Category Confusion Table

True	Classified as Percent (%)				
Category	C	F	P	U	W
C	0.00	10.42	66.59	0.00	22.99
F	0.00	61.86	14.90	4.09	19.15
P	0.00	6.99	76.61	0.07	16.33
U	0.00	58.27	7.01	22.84	11.88
W	0.00	12.01	58.32	0.00	29.66

Weighted Overall Classification Accuracy = 49.86%

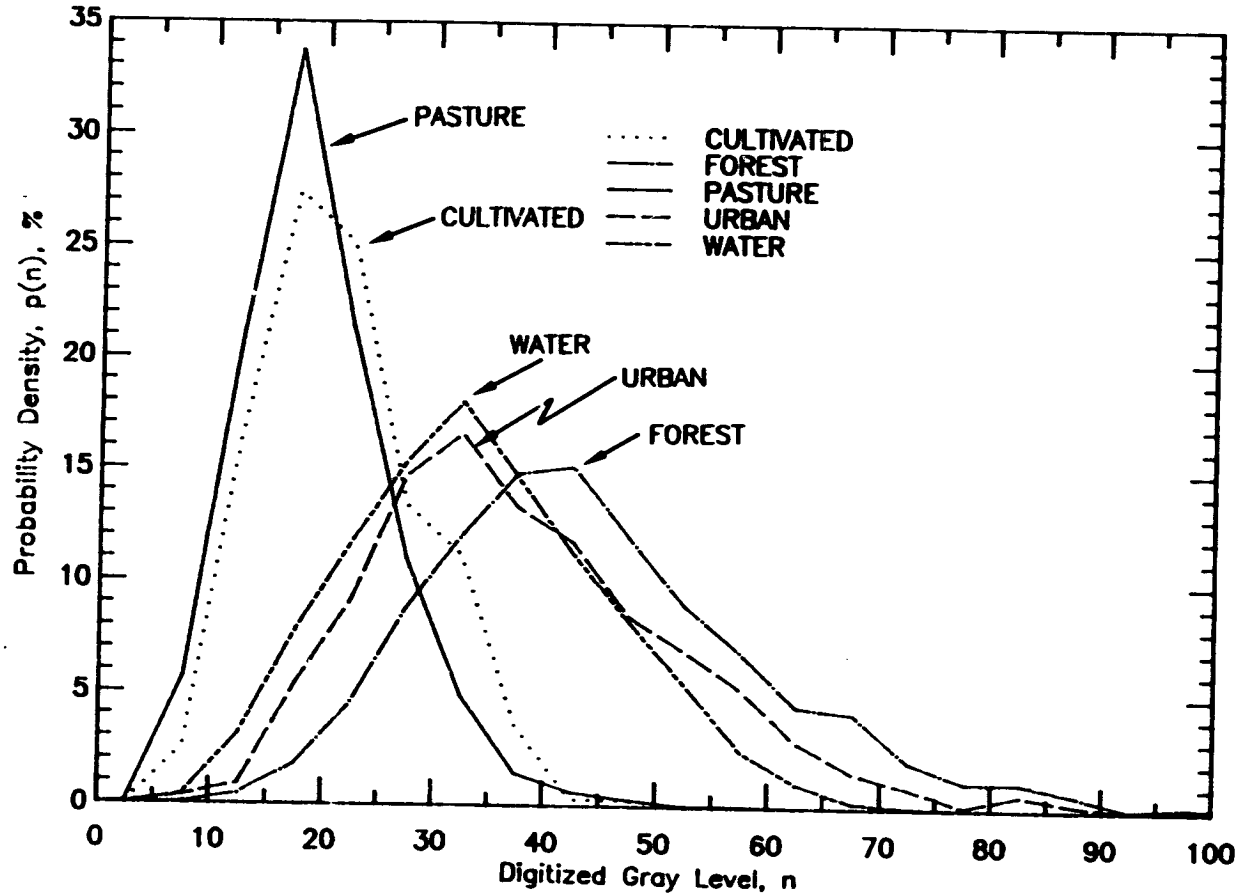

Fig. 3.6. Standardized probability density distribution of gray level for Seasat (Aug. 20, Rev. 774) ascending-pass training pixels of the land-cover classification study area.

TABLE 3.3

Category Confusion Table and Separability Measures of the Supervised Maximum-Likelihood Classification for Seasat (Rev. 795) Pixel Data for the Categories Cultivated (C), Forest (F), Pasture (P), Urban (U), and Water (W)

	Category				
	C	F	P	U	W
Mean	22.18	44.89	19.83	39.01	34.33
Std. Dev.	7.11	15.10	6.87	15.07	11.42

Separability

C-F	C-P	C-U	C-W	F-P	F-U	F-W	P-U	P-W	U-W
1.02	0.17	0.76	0.66	1.14	0.20	0.40	0.87	0.79	0.18

Category Confusion Table

True	Classified as Percent (%)				
Category	C	F	P	U	W
C	0.00	3.01	78.34	0.00	18.65
F	0.00	65.73	10.52	0.00	23.74
P	0.00	2.08	66.67	0.00	11.25
U	0.13	50.20	20.53	0.00	29.13
W	0.00	31.45	28.67	0.00	33.88

Weighted Overall Classification Accuracy = 50.32%

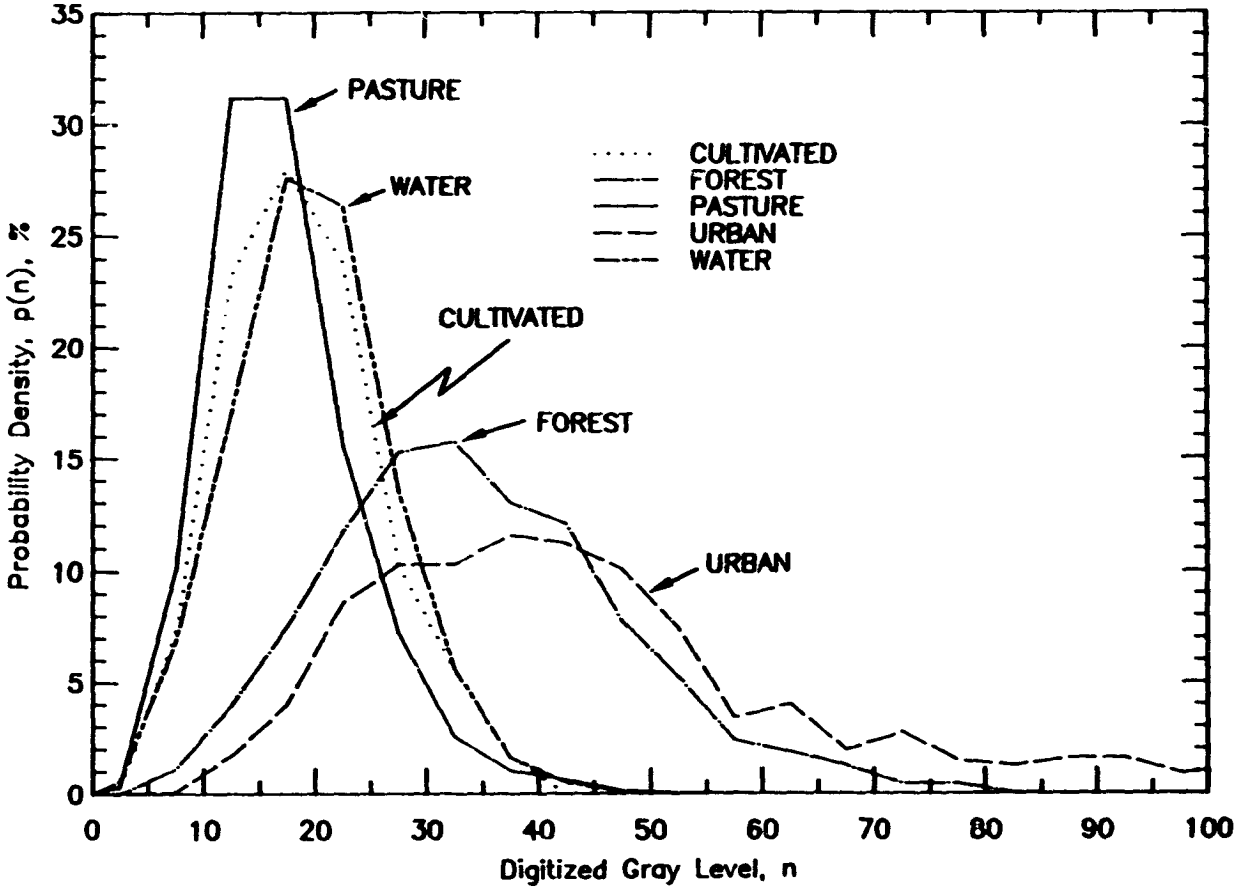

Fig. 3.7. Standardized probability density distribution of gray level for Seasat (Aug. 21, Rev. 795) descending-pass training pixels of the land-cover classification study area.

compared to the descending pass such that they overlapped with the urban and forest pixels rather than with the cultivated and pasture pixels. Furthermore, the urban pixels were not as bright on the ascending pass as they were on the descending pass. This resulted in a decreased classification accuracy for urban pixels (≈ 23% to 0%) and an increased classification accuracy for pasture pixels (≈77% to 87%). The other categories yielded similar classification accuracies.

The SIR-A pixel data resulted in a weighted overall classification accuracy of 71.79%. This is a considerable improvement over the results obtained with the Seasat data, and upon examination of the classification attributes (Table 3.4, Figure 3.8), it can be related to two causes. First, the pixels in the water category have a much lower return than they do on the Seasat images relative to other target classes, and thus they are classified more accurately (i.e., from 34% to 94%). Secondly, in the SIR-A image, the forest and urban pixels are proportionately much brighter than the pixels in the other categories when compared to the Seasat images. This results in an improved classification accuracy of approximately 63% to 95% for the forest category. Cultivated pixels are entirely misclassified, being most often identified as pasture or water pixels. Urban pixels (1.93% accuracy) are almost entirely classified as forest pixels, whereas pasture pixels are correctly identified 70% of the time, which is close to the accuracy obtained on the descending Seasat pass.

TABLE 3.4

Category Confusion Table and Separability Measures for the SIR-A Supervised Maximum-Likelihood Pixel Classification for the Categories Cultivated (C), Forest (F), Pasture (P), Urban (U), and Water (W)

	Category				
	C	F	P	U	W
Mean	48.24	188.82	59.53	198.18	32.31
Std. Dev.	12.27	51.58	21.76	62.89	5.88

Separability

C-F	C-P	C-U	C-W	F-P	F-U	F-W	P-U	P-W	U-W
2.20	0.27	2.00	0.88	1.79	0.08	2.72	1.66	0.91	2.41

Category Confusion Table

True	Classified as Percent (%)				
Category	C	F	P	U	W
C	0.00	1.86	55.23	0.00	42.91
F	0.00	95.18	3.43	1.39	0.00
P	0.00	6.58	70.16	0.00	23.26
U	0.00	95.42	2.65	1.93	0.00
W	0.00	0.03	6.15	0.00	93.82

Weighted Overall Classification Accuracy = 71.79%

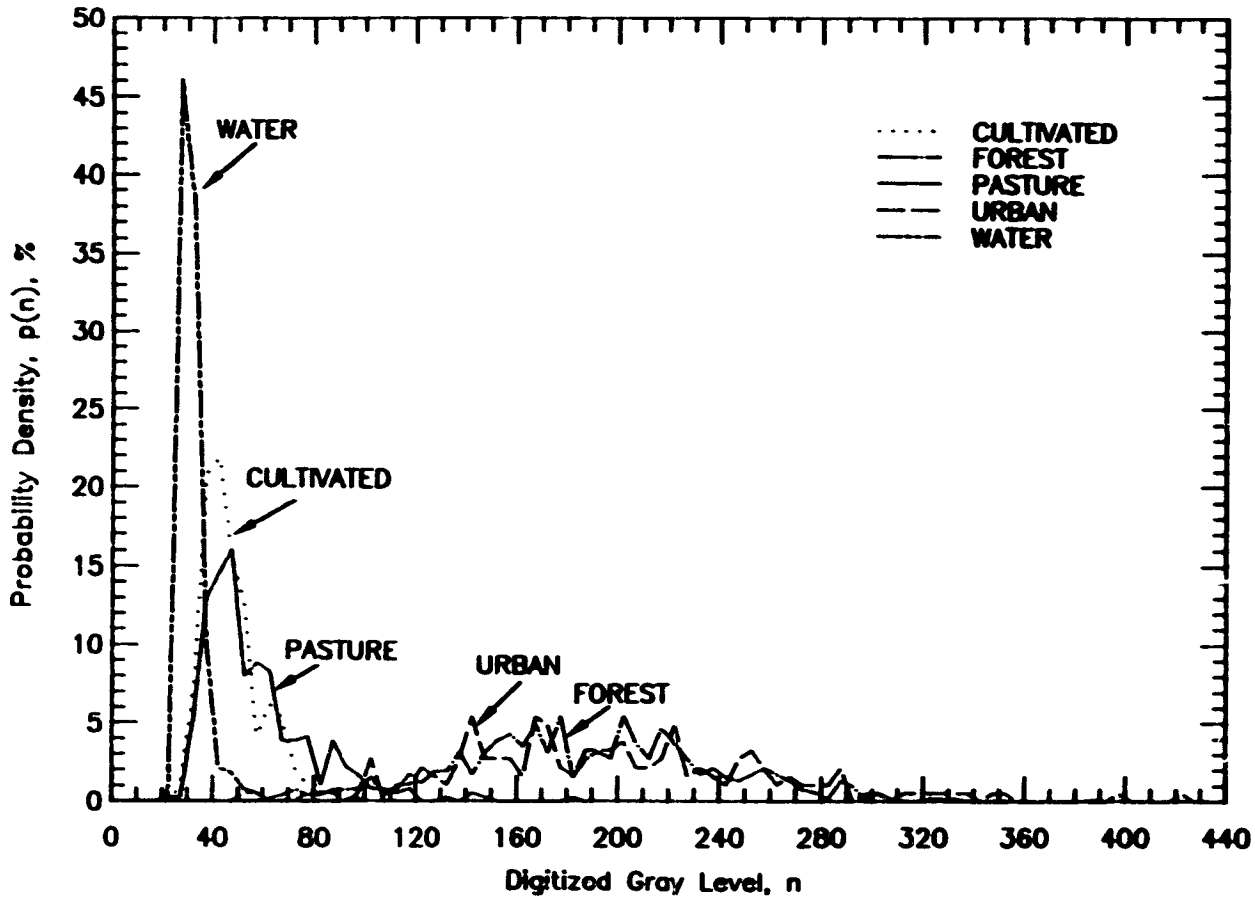

Fig. 3.8. Standardized probability density distribution of gray level for SIR-A pass (Nov. 13, 1982) training pixels of the land-cover classification study area.

Per-pixel supervised classification of data from Landsat bands 5 and 7 produced a weighted overall classification accuracy of 62.26% (Table 3.5), which is intermediate in accuracy between that obtained with the Seasat and with the SIR-A data. Water is perfectly classified with the Landsat data, largely because of the very low reflectance values on band 7. Pixels in the cultivated category are accurately identified 92% of the time due to high reflectances in bands 5 and 7. This is a great improvement over the SAR data, in which cultivated pixels were never accurately identified. Pixels in the forest and urban categories are identified with accuracies of 70.4 and 66.5%, respectively. There is a high degree of confusion between forest, urban, and pasture pixels, the latter being poorly classified (accuracy = 28.1%). Given that these cover types are composed of various combinations of trees, grass, and buildings, this result is not unexpected.

Microwave backscattering from terrain elements is a function of the system parameters and of the dielectric and geometric characteristics of the target. The general response of the land-cover categories as observed on the SAR imagery is typical of these types of targets at L-band frequencies. The orthogonal look directions of the two Seasat images results in different backscattering characteristics for the water and urban categories. This difference in tone may be related to the orientation of residential street patterns, i.e., it may be similar to the cardinal effect reported by Hardaway et al. (1982). For the water category, the wind direction and resulting surface roughness in relationship to look direction are the

TABLE 3.5

Category Confusion Table for the Supervised Maximum-Likelihood Pixel Classification of Landsat Data (Bands 5 and 7) for the Categories Cultivated (C), Forest (F), Pasture (P), Urban (U), and Water (W)

Category Confusion Table

True Category	Classified as Percent (%)				
	C	F	P	U	W
C	92.2	0.0	2.9	4.0	0.0
F	0.0	70.4	4.1	25.6	0.0
P	3.0	29.1	28.1	39.7	0.0
U	0.0	15.0	18.5	66.5	0.0
W	0.0	0.0	0.0	0.0	100.0

Weighted Overall Classification Accuracy = 62.26%

probable causes of the difference in tone observed in the two images.

The effect of the different incidence angles of the two SAR systems (20° for Seasat versus 50° for SIR-A) also influences the nature of the backscattering for the water category. Water acts as a specular reflector, and at the 50° SIR-A incidence angle, it yields little backscattering, thus allowing accurate discrimination (99% accuracy). At the 20° Seasat incidence angle, however, water exhibits more backscattering, which is probably attributable to wind-induced surface roughness. The increased backscattering led to a brighter tone for the water pixels on the Seasat images and thus increased confusion with the pasture and forest categories. Another, although more subtle, difference caused by the changing incidence angle was the backscattering from the forest and urban cover-types. In the Seasat images, more noticeably on the descending pass, the urban pixels are relatively brighter than the forest pixels. At a 50° incidence angle, the microwaves may undergo more attenuation in a forest canopy than in urban cover, which may explain the lower return characteristic of forests.

3.5 Spatial Averaging and Multisensor Classification

Spatial averaging of the pixels within a field resulted in increased classification accuracy (~10%) for both SIR-A data and Seasat data (Rev. 774). The increase in accuracy is rapid at first, until about 20 independent samples (N) are averaged, at which point the increase in accuracy becomes gradual

(Figure 3.9). The averaging of five pixels for the Seasat data, which were processed at four looks, produces 20 independent samples, whereas for the SIR-A data (six looks) it represents the averaging of three to four pixels. The author attributes the initial rapid increase in classification accuracy to a reduction in fading and the more gradual increase at higher values of N to the averaging of within-field variability as well as to a further reduction in fading. Spatial averaging of the Landsat data with a 6 x 6 filter resulted in an increased classification accuracy of only 4.1% (i.e., from 62.3% to 66.4%). This is largely due to the averaging of within-field variability, as the time-bandwidth product of the Landsat data is large enough to make the consequences of fading insignificant.

The multisensor combinations were classified on a per-field basis, since there was no attempt to register the different data sets on a per-pixel basis. Due to the fact that some fields were either too small or could not be identified on the Landsat imagery, only 32 of the original 40 fields were used in these analyses. The results of the multisensor, supervised classification are summarized in Figure 3.10. Note that the base level in each multisensor classification in Figure 3.10 is the accuracy achieved with a 6-pixel by 6-pixel, spatially averaged data set.

Combining Landsat bands 5 and 7 with each SAR data set did not improve classification accuracy as much as combining the two Seasat data sets, nor as much as when the Seasat data were combined with the SIR-A data. This was largely due to the

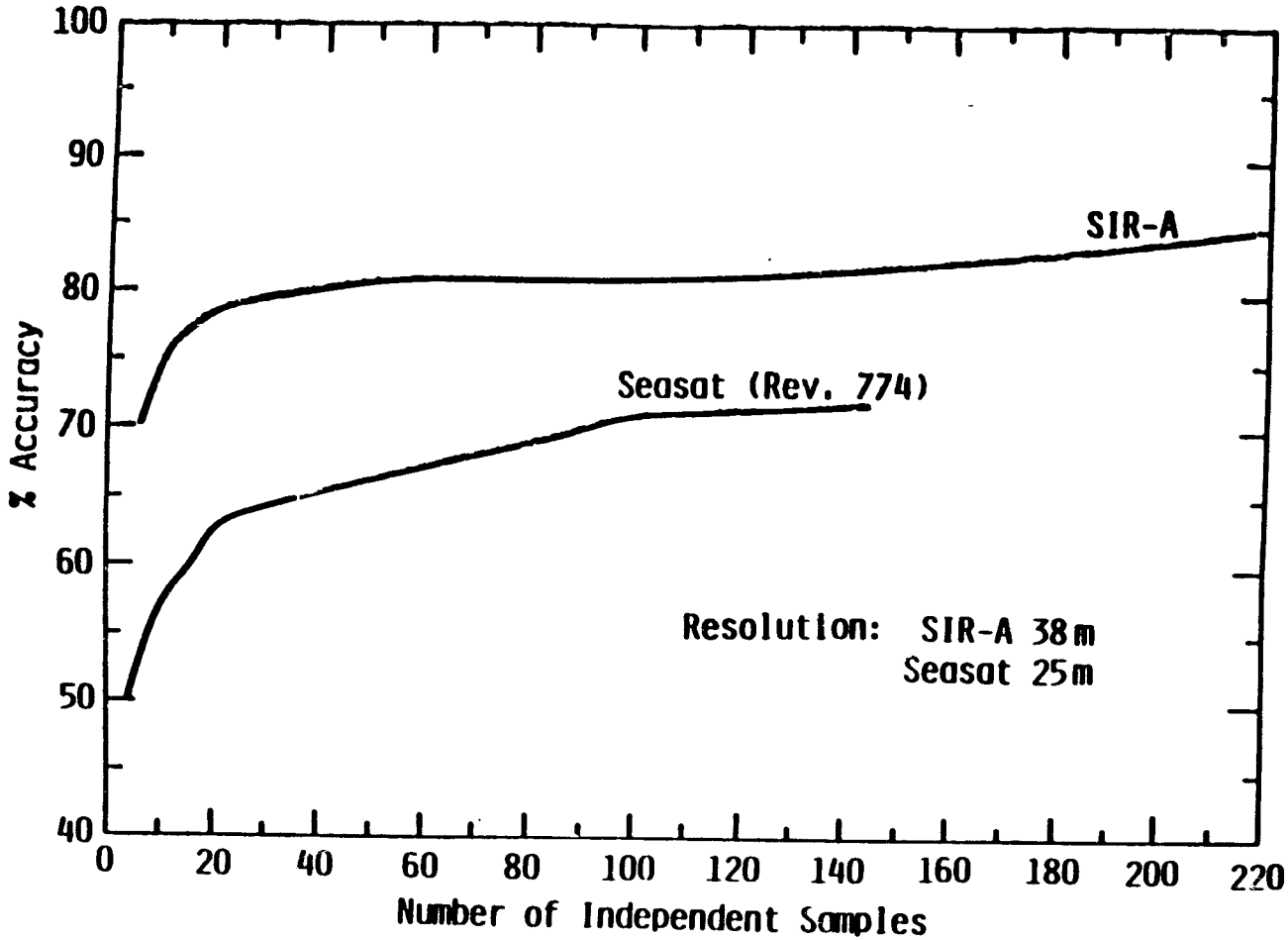

Fig. 3.9. The effects of averaging independent samples (N) upon the classification accuracy of both Seasat (Aug. 20, Rev. 774) and SIR-A (Nov. 13) data.

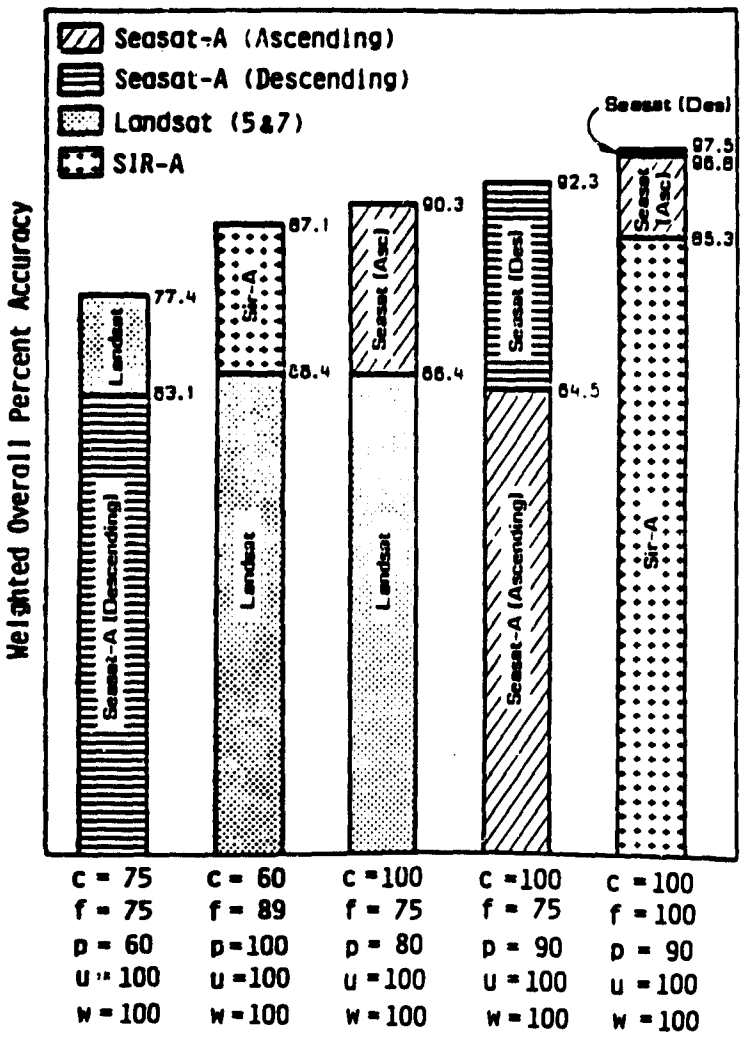

Fig. 3.10. Summary of multisensor supervised land-cover classification results for the Oklahoma study area. Note that the lower level of each bar is the classification accuracy achieved with a six-pixel, spatially averaged data set.

confusion of forest with pasture fields that occurred when using the combined MSS and SAR data. However, all multisensor combinations produced higher classification accuracies than any single channel, with the best results obtained by combining SAR data obtained at different incidence angles.

The best weighted overall classification accuracy (97.5%) was achieved by combining the two Seasat data sets with the SIR-A data (Table 3.6). Note that the combination of the ascending Seasat data with the SIR-A data results in a 96.8% classification accuracy, with the addition of the descending Seasat data improving the accuracy only 0.7%. When all three SAR data sets were combined, all categories were classified with 100% accuracy, with the exception of pasture fields. Ten of the pasture fields were confused with cultivated fields, resulting in a 90% classification accuracy for the pasture category.

Previous research has demonstrated the complementary nature of MSS data and SAR data (Ahern et al., 1978; Wu, 1980; Ulaby et al., 1982). The per-pixel classifications reported in this study also indicated that an MSS and SAR data combination would do very well at discriminating these five cover types, since the highly confused categories were different for the MSS data as compared to the SAR data. In view of these results, further research needs to be conducted to investigate the synergistic nature of satellite MSS and SAR data. Further improvements in classification accuracy can also be expected by using multitemporal data (Brisco and Protz, 1980; Bush and Ulaby, 1978; Paris, 1982; Shanmugan et al., 1983) and incorporating a machine measure of texture into the

TABLE 3.6

Category Confusion Table for the Supervised Maximum-Likelihood Classification of the Combined SIR-A Data and Seasat Ascending and Descending Passes

Category Confusion Table

True Category	Classified as Percent (%)				
	C	F	P	U	W
C	100.0	0.0	0.0	0.0	0.0
F	0.0	100.0	0.0	0.0	0.0
P	10.0	0.0	90.0	0.0	0.0
U	0.0	0.0	0.0	100.0	0.0
W	0.0	0.0	0.0	0.0	100.0

Weighted Overall Classification Accuracy = 97.99%

classification algorithm (Berger, 1980; Haralick et al., 1970).

The SIR-A and Seasat sensors were designed for geologic and oceanographic applications, respectively. Nonetheless, the imagery of land surfaces produced by the SAR systems has demonstrated the usefulness of space-radar data for other terrain applications. The results presented above indicate that incidence angle significantly influences radar land-cover discrimination capabilities when comparing SIR-A and Seasat data. As orbital SAR data with varying incidence angles are acquired during the SIR-B experiments, it is likely that further insight into the influence of incidence angle on microwave remote sensing will be gained.

3.6 Summary

Supervised maximum-likelihood classifications of Seasat, SIR-A, and Landsat (bands 5 and 7) pixel data demonstrated that SIR-A data provided the most accurate discrimination (72%) of five land-cover categories. The spatial averaging of the SAR data improved classification accuracy significantly as a result of a reduction in signal fading and because of the averaging of the within-field variability. Some improvement in classification accuracy was obtained by averaging the Landsat data. This was attributed to reduced within-field variability. The results of using various multisensor combinations indicated that the best classification accuracy was achieved by combining SAR data obtained at different incidence angles. The best multisensor classification accuracy (97.5%) was achieved by combining ascending and descending Seasat data sets with SIR-A data. Other

investigators have reported significant improvements using MSS data combined with SAR data. As more space SAR data become available, additional research should be conducted to investigate further the possibility of land-cover classification using multiple sensors.

CHAPTER 4

CROP CLASSIFICATION IN KANSAS

4.1 Introduction

In the previous chapter, Level I land-cover classification (Anderson et al., 1976) using satellite SAR and MSS data was investigated. The results were very promising, indicating that a satellite remote-sensing system may be capable of mapping land cover at this level of classification. For many applications, however, a more detailed level of discrimination is necessary.

It has been suggested that remote sensing offers great potential for mapping and monitoring agricultural production (Bauer, 1975). The first step in the process is the accurate identification of the various crop types found in a particular region. Toward this end, it has been shown that multitemporal MSS data can identify crops accurately (Lacie Symposium, 1978). However, the problem of interrupted coverage caused by weather conditions still exists when using multispectral scanner data, and the severity of the problem varies with location. As a result, there is continuing interest in using the microwave portion of the electromagnetic spectrum to alleviate this difficulty.

Previous studies have determined that crop-type influences radar return and that discrimination is therefore possible (Simonett et al., 1967; Schwarz and Caspall, 1968; Haralick et al., 1970). The variations in plant geometry and moisture content characteristic of different crop types lead to

differences in the backscattering coefficient, which allows discrimination to occur. Section 2.4 provides a review of the research investigating crop discrimination with radar.

No studies have yet been conducted using satellite SAR data for crop-discrimination purposes. Although the system parameters of Seasat are not optimum for crop classification, multitemporal data sets from Seasat are available and are amenable to crop-discrimination research. This chapter presents findings based on Seasat SAR data, both alone and in combination with Landsat data, for crop classification. Multichannel combinations consisting of multidate SAR data and multisensor data were used for the maximum-likelihood classification of corn, milo, and wheat.

4.2 Image Data and Test-Site Description

The Garden City area of western Kansas was imaged several times during the 1978 growing season by the Seasat SAR. Digitally processed images from three ascending orbital tracks were acquired over this site. The images were recorded on September 22 (Rev. 1254), October 1 (Rev. 1383), and October 7 (Rev. 1469), 1978.

An analysis of the radiometric stability of these three Seasat scenes revealed that the September 22 and October 7 images are equivalent, whereas the October 1 scene shows a consistent gain bias that is 1.7 dB below the other two images (Brisco et al., 1983). A Landsat CCT of an October 14 scene of the same area (# 30223-16911) was also obtained. The area at

which these four images overlapped was used as the study area (Figure 4.1).

The area south of the Arkansas River is intensively irrigated, largely by center-pivot sprinkler systems. Corn, milo, and wheat are the crops most commonly grown in the region, with occasional fields of Sudan grass, sugarbeets, and alfalfa also present. An inventory of the field types occurring in the area in 1978 was compiled from aerial photographs provided by the Agricultural Stabilization and Conservation Service (ASCS) (the ASCS acquires such images for crop-inventory purposes).

For several reasons, it was decided to limit the study to center-pivot fields of corn, milo, and wheat. First, only these crop types were represented by a sufficiently large number of fields to be included in subsequent classification analyses. Next, these three crops were the most important cash crops grown in the region. Finally, the boundaries of the center-pivot fields were distinct on the imagery, and thus confidence was imparted to the registration of the image data to the field inventory. The Seasat images used in the crop-classification analyses are presented in Figures 4.2 through 4.4; band 5 from the Landsat scene is depicted in Figure 4.5.

4.3 Methodology

Ten center-pivot fields each of corn, milo, and wheat were identified on the imagery. The corner-point coordinates of these 30 fields were then obtained for each image, using the VDI image-analysis system. These data were then extracted from the

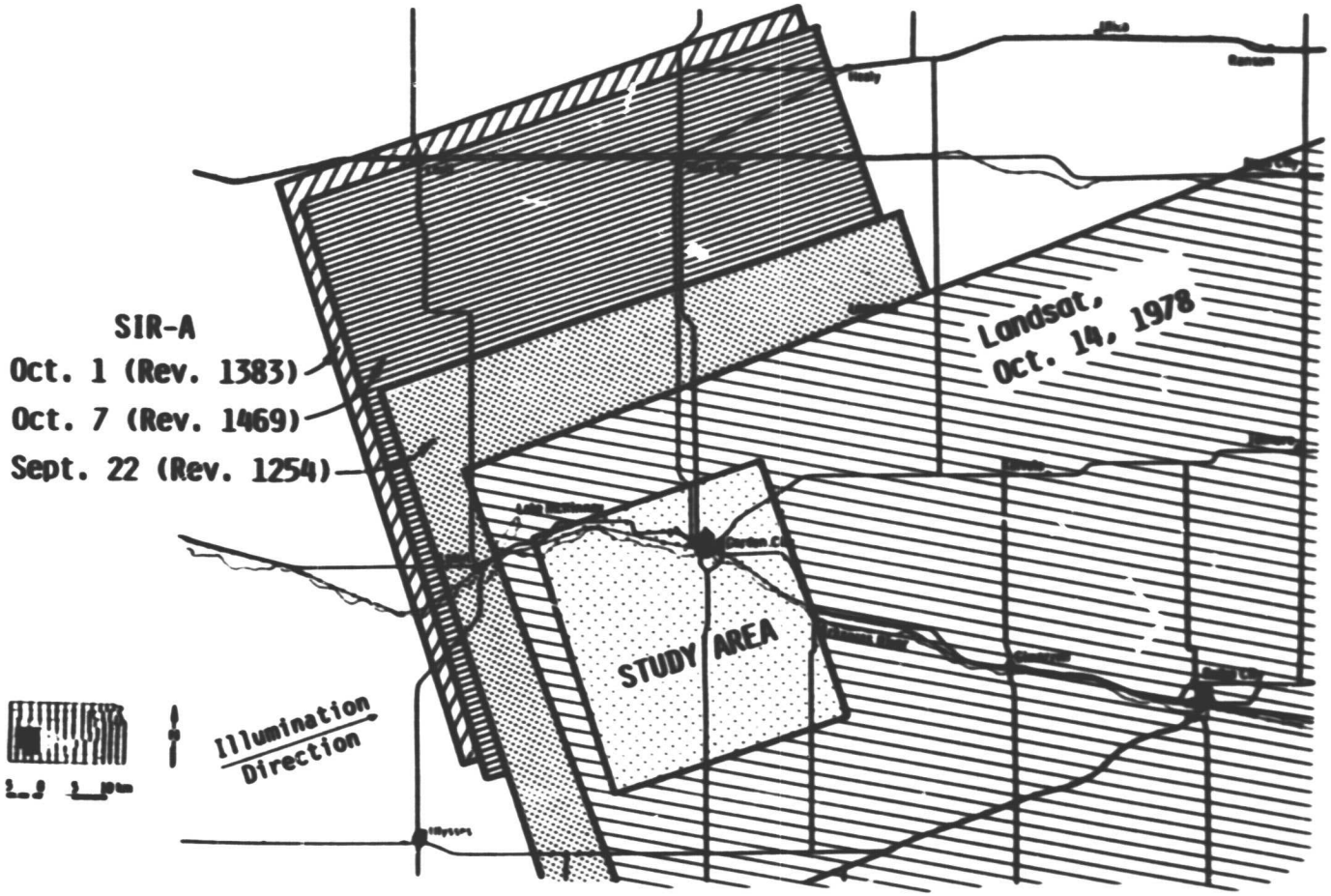

Fig. 4.1. Geographic locations corresponding to the Seasat and Landsat images used in the Kansas crop-classification study.

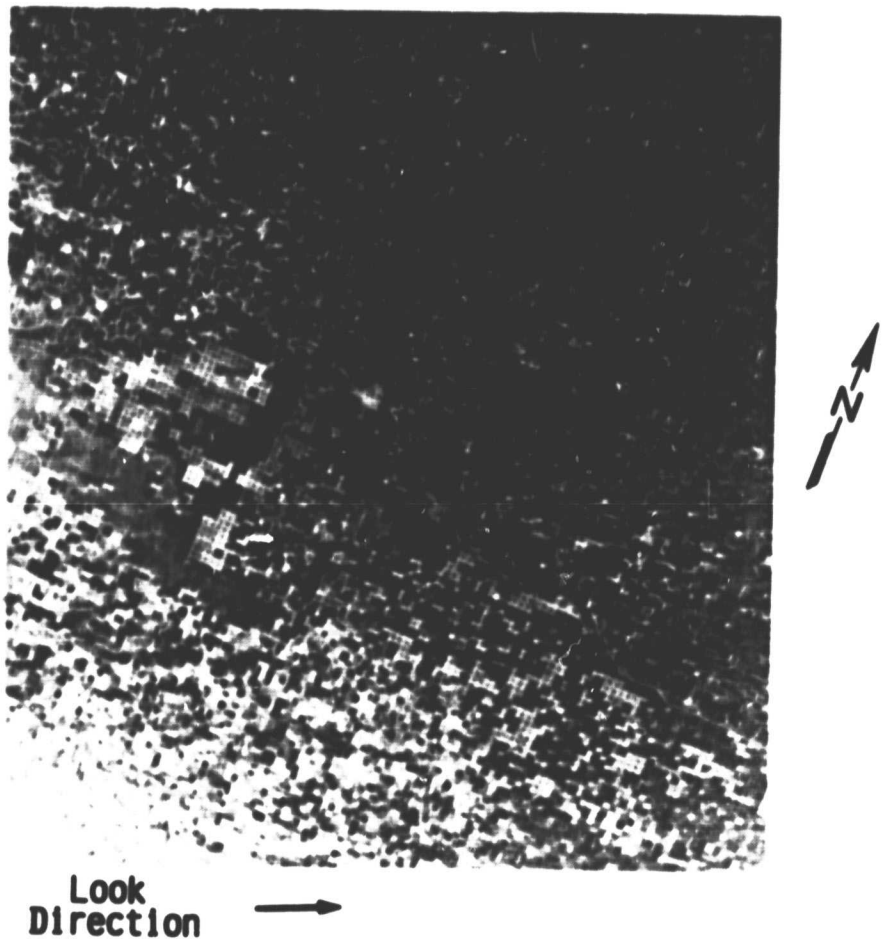

Fig. 4.2. September 22 Seasat image of the Kansas crop-classification study area.

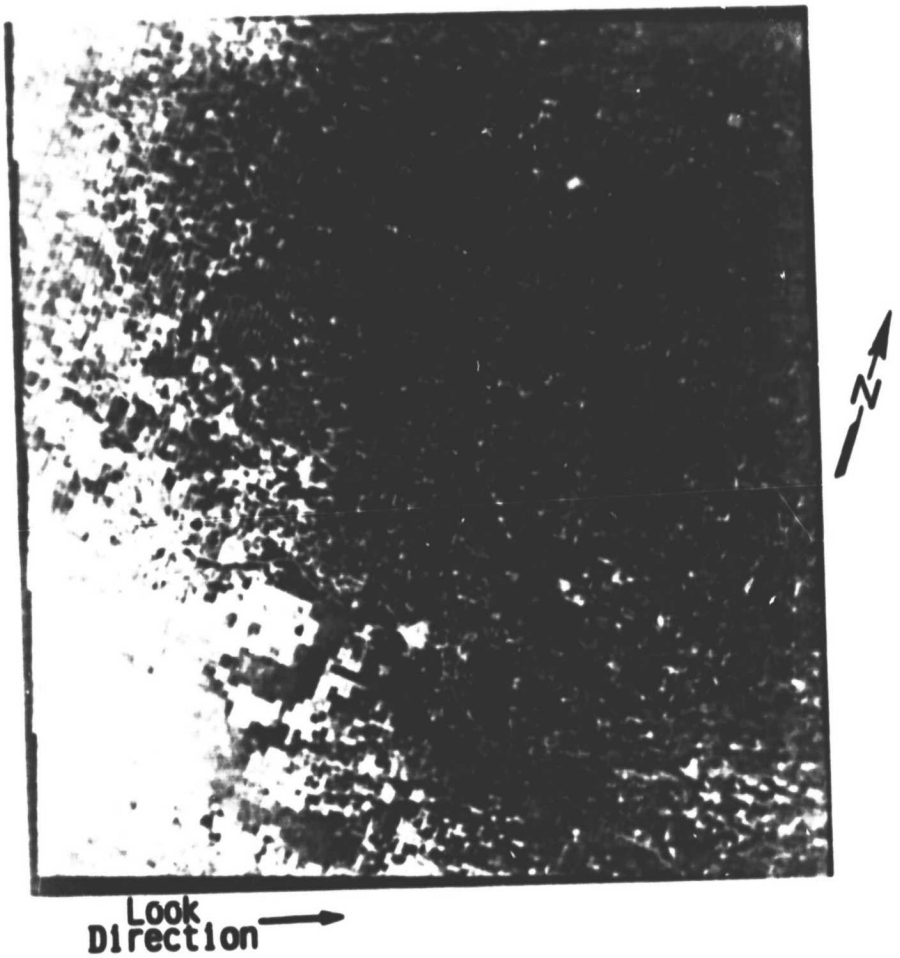

Fig. 4.3. October 1 Seasat image of the Kansas crop-classification study area.

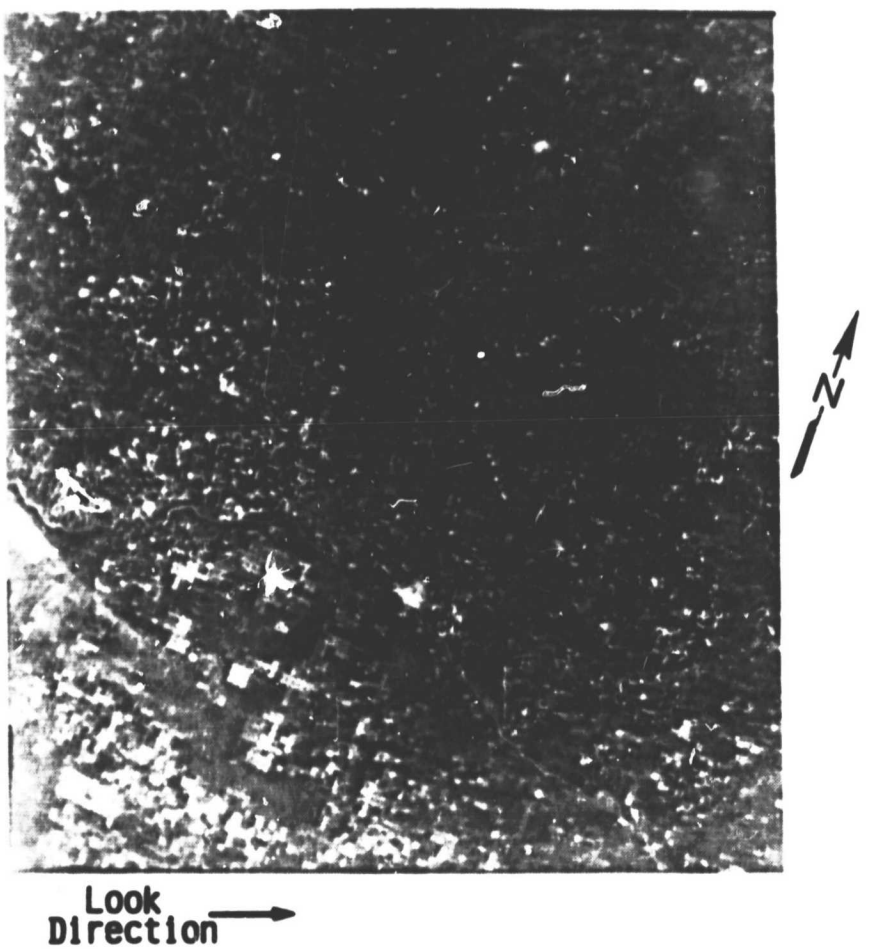

Fig. 4.4. October 7 Seasat image of the Kansas crop-classification study area.

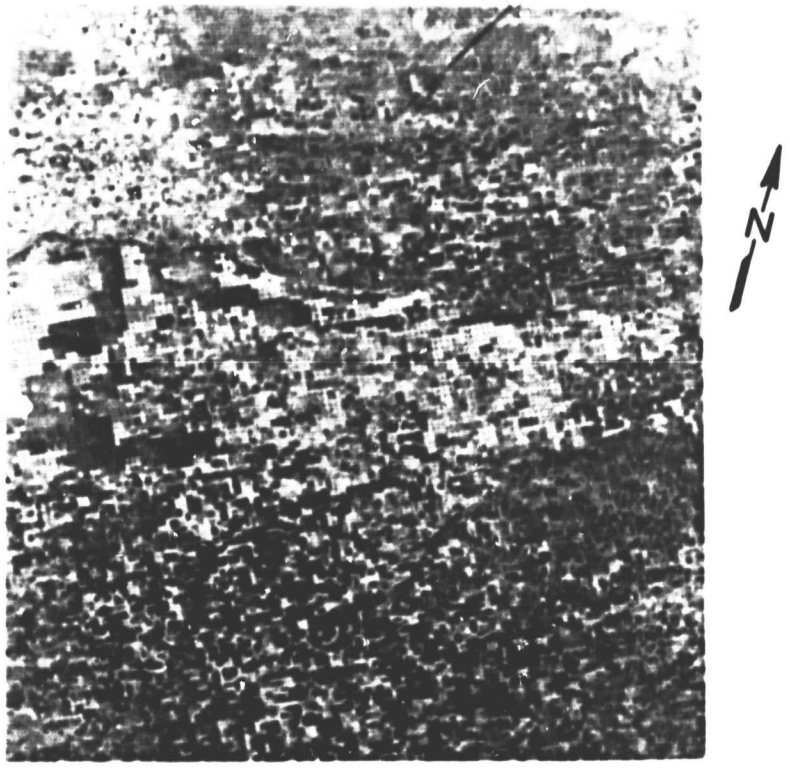

Fig. 4.5. Landsat band 7 (October 14, 1978) image of the Kansas crop-classification study area.

image tapes and subjected to the MLC routine used in the analysis reported in Chapter 3.

Per-pixel classifications were first performed on each data set using a 10%-training and 90%-testing s[illegible]. The image data were averaged, using a 6 x 6 window for the Seasat data and a 4 x 4 window for the Landsat data, and then reclassified using the same training and testing sample sizes.

Next, the Landsat data files were rotated 90° to the left to match the orientation of the Seasat images and to allow registration of the two data files. The data were also edited as necessary to produce the same number of averaged pixels per field. All multidate combinations of Seasat SAR data were classified using the MLC routine, and classifications of the spatially averaged data were performed on various combinations of the Seasat and Landsat data. For the multichannel classifications, a 20%-testing and 80%-training sample was used.

4.4 Single-Channel Classification

The per-pixel classifications and the classifications performed on the averaged data are presented in Table 4.1. An improvement in classification accuracy of approximately 10% was achieved by averaging the Seasat data, whereas little change occurred in the Landsat classifications. For the Seasat data, this is attributed to a reduction in fading, (Bush and Ulaby, 1975), whereas for the Landsat data the time-bandwidth product was large enough to make the consequences of fading insignificant. The Seasat data started as an average of four

TABLE 4.1

Category Confusion Tables for the Per-Pixel Classifications and for Classifications of the Averaged Data for Corn (C), Milo (M), and Wheat (W)

Channel	True Category	Pixel Classified as C	M	W		Averaged Data Classified as C	M	W
Sept. 22 Seasat	C	50.2	32.6	17.2	C	47.2	51.9	.9
	M	24.1	39.0	36.9	M	14.6	73.9	11.6
	W	2.3	18.4	79.2	W	0.0	19.2	80.8
			T.A.* = 56.15				T.A. = 66.94	
		C	M	W		C	M	W
Oct. 1 Seasat	C	37.4	28.1	34.5	C	64.7	25.9	9.4
	M	31.6	31.4	36.9	M	49.4	43.3	7.3
	W	9.0	16.6	74.4	W	15.9	19.4	64.7
			T.A. = 47.27				T.A. = 57.34	
		C	M	W		C	M	W
Oct. 7 Seasat	C	45.6	28.9	25.6	C	47.9	31.9	20.1
	M	20.9	38.3	40.8	M	11.1	50.7	38.2
	W	5.6	21.9	72.4	W	1.4	16.2	82.4
			T.A. = 52.01				T.A. = 60.55	
		C	M	W		C	M	W
Landsat 5	C	77.0	14.7	8.4	C	54.2	14.6	31.3
	M	55.3	36.1	8.6	M	34.0	34.0	31.9
	W	62.7	24.3	13.0	W	36.1	22.9	41.0
			T.A. = 42.50				T.A. = 43.06	
		C	M	W		C	M	W
Landsat 7	C	76.3	12.5	11.2	C	81.3	6.3	12.5
	M	55.5	27.3	17.2	M	58.3	27.1	14.6
	W	54.9	25.7	19.4	W	54.2	19.4	26.4
			T.A. = 41.60				T.A. = 44.91	

* T.A. = Total Accuracy

looks, such that the 6 x 6 average represents 144 looks.

The Seasat data always produced higher classification accuracies than the Landsat data. Of the three Seasat scenes, the September 22 scene produced the highest classification accuracy (67%), followed by the October 1 scene (57%). Wheat was always the most accurately identified crop, followed by milo on September 22 and October 7, and corn on October 1. Landsat band 5 produced a 43% correct classification, whereas a 45% correct classification was achieved using band 7. Bands 4 and 6 were not included in the analysis because they are very highly correlated with bands 5 and 7, respectively. When the Landsat data were used, corn was the most accurately identified crop. The statistics for the three crop types from all five channels are presented in Table 4.2; Figure 4.6 is a graphical presentation of both the means and the standard deviations. The figure, along with a generalized crop calendar (Figure 4.7), is useful in explaining the classification results.

In late September and early October, the corn was being harvested, whereas milo was just reaching maturity. The winter-wheat fields were harvested in late June or early July and were either lying fallow at that time of year or being replanted. Thus, on the Seasat imagery, wheat fields are always dark in tone, whereas corn and milo are brighter. This results in the high confusion between corn and milo (see Figure 4.6), whereas the wheat fields are more accurately discriminated. Ulaby et al. (1979) also reported milo as being the worst-classified crop; it was often misclassified as corn.

TABLE 4.2

Statistics for the Three Crop Types from all Five Channels Used in the Classification Analyses

Channel	Statistic	Corn	Milo	Wheat
Seasat: Sept. 22	Mean	41.10	32.25	22.00
	Std. Dev.	9.19	4.75	3.79
	Minimum	24.41	24.06	15.06
	Maximum	75.53	48.78	34.78
	Range	51.12	24.72	19.72
Seasat: Oct. 1	Mean	27.54	24.50	17.73
	Std. Dev.	6.30	4.52	4.39
	Minimum	16.75	16.97	11.47
	Maximum	51.17	38.86	34.03
	Range	34.41	21.89	22.56
Seasat: Oct. 7	Mean	32.23	24.73	18.81
	Std. Dev.	11.38	4.62	4.47
	Minimum	16.42	16.61	12.31
	Maximum	77.08	44.25	36.92
	Range	60.66	27.64	24.61
Landsat: Band 5	Mean	30.46	34.53	32.27
	Std. Dev.	4.98	10.02	7.71
	Minimum	21.00	16.75	21.00
	Maximum	50.50	54.50	50.00
	Range	29.50	37.75	29.00
Landsat: Band 7	Mean	18.69	22.30	20.91
	Std. Dev.	3.17	5.50	4.43
	Minimum	14.75	15.00	13.75
	Maximum	31.50	33.50	30.75
	Range	16.75	18.50	17.00

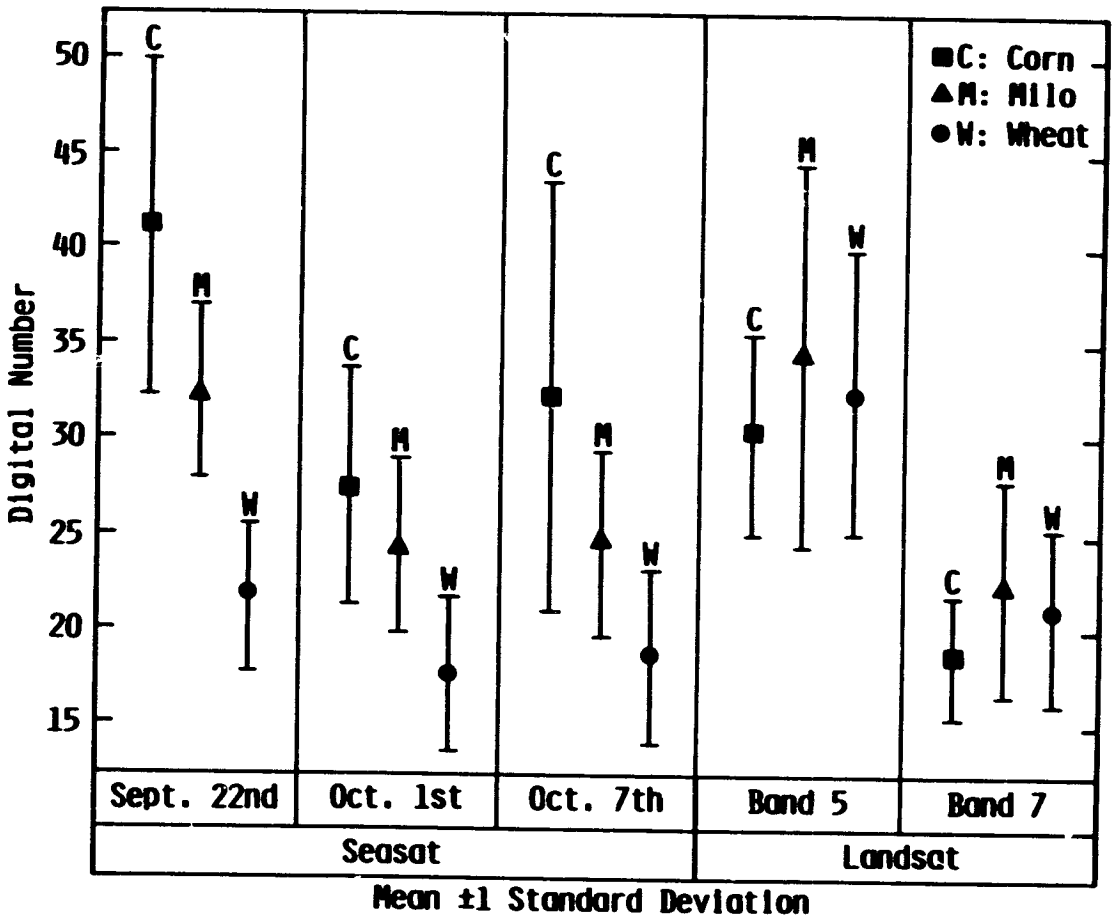

Fig. 4.6. Graphical presentation of the means and standard deviations of the crop types for the classification study.

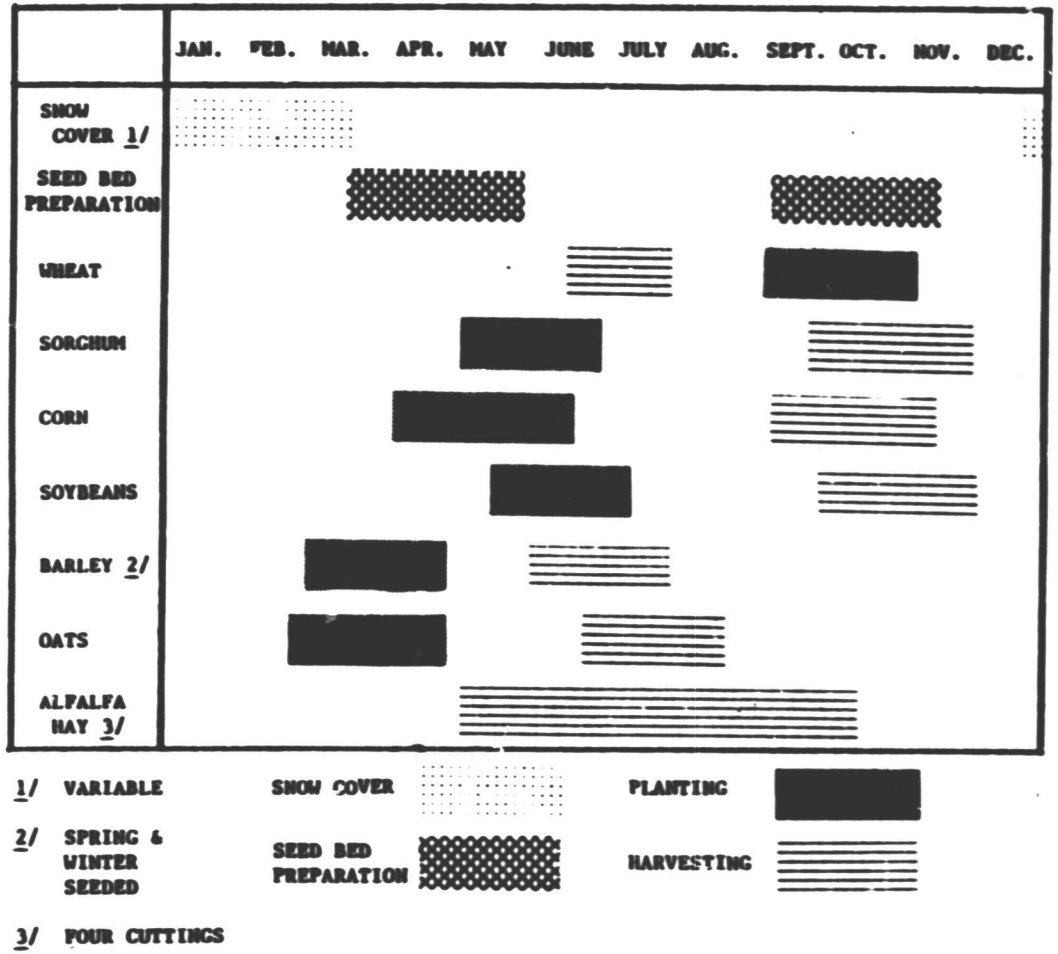

Fig. 4.7. Generalized crop calendar for the area of Kansas used in the crop-classification study.

Landsat band 5 responds to the chlorophyll content (levels) of the plants, whereas band 7 responds to the plants' cell structure. The milo was still somewhat green and turgid during the time period of this study and thus produced higher reflectances in band 7. Based on the Landsat data, corn was likely to be the most accurately identified crop because of the very low IR reflections resulting from plant senescence. Due to the withered state of the canopies, the soil background also may have been important in the interpretation of reflectances in the visible region. For example, the study area was dominated by sandy soils, with relatively little variability in soil type, which tended to decrease the differences in reflectance in the visible region for these three crop types due to the similar structure and composition of the underlying soils.

The accurate classification of corn using radar data has been reported in at least two previous studies (Brisco and Protz, 1980; Shanmugan et al., 1983). However, these studies made use of only two radar frequencies and did not include milo as a category. The high confusion reported previously between corn and milo is understandable given the similar physical appearances and growing seasons of the two crops. A more detailed crop calendar for corn and milo is presented in Table 4.3. On the images, the overlapping in maturity and harvest dates increases the confusion between the two crops. The large amount of vegetation biomass in either a corn field or a milo field results in a large σ^{o} for these crops and thus produces a bright return on the image. The wheat fields contain

TABLE 4.3

Maturity and Harvest Dates for Corn and Milo;
Percent of Acreage by Specified Dates for the
Southwest Crop Reporting Unit of Kansas
(Average of 1973-1977)

	September			October		
	10	20	30	10	20	30
Corn maturity	30	45	75	90	95	100
Corn harvest	0	5	15	30	55	70
Milo maturity	10	20	45	75	85	95
Milo harvest	--	--	5	15	30	50

little vegetation and thus have a low σ^{o} in the Seasat data; consequently, they are accurately identified. However, if the classifications are performed for the whole scene, large errors of commission for wheat from areas such as grasslands and heavily utilized pasture can be expected.

4.5 Multichannel SAR Classification

Multidate SAR classifications are presented in Table 4.4. By using the data from September 22 in combination with either the data from October 1 or October 7, a classification accuracy of approximately 75% was achieved. This represents an 8% increase over the best single-channel classification accuracy (67%) achieved using the September 22 data. Combining data from the October dates produced about the same accuracy (66%) as that achieved using the September 22 date alone. The three-date combination performed similarly to a two-date combination that included September 22, with an accuracy of 74.48%.

The two-date SAR combinations improved the wheat classification accuracy in both cases. Corn classification accuracy improved more for the September 22/October 7 combination, whereas the September 22/October 1 combination resulted in the greatest improvement in the classification of milo. Once again, the data in Figure 4.6 illustrate why these improvements occurred. Wheat produced the lowest return in all cases; thus, any two-date combination enhanced wheat classification. The corn data of October 7 had a relatively higher mean, compared to milo, than the October 1 data; thus,

TABLE 4.4

Category Confusion Tables for the Multidate SAR Classifications of Corn (C), Milo (M), and Wheat (W)

September 22/October 1

	C	M	W
C	52.3	46.1	1.6
M	8.6	82.8	8.6
W	0.0	10.9	89.1

T.A.* = 74.74

September 22/October 7

	C	M	W
C	60.9	38.3	0.8
M	13.3	74.2	12.5
W	1.6	9.4	89.1

T.A. = 74.74

October 1/October 7

	C	M	W
C	53.1	43.0	3.9
M	19.5	68.0	12.5
W	4.7	18.8	76.6

T.A. = 65.89

September 22/October 1/October 7

	C	M	W
C	66.4	32.8	.8
M	17.2	80.5	2.3
W	6.3	17.2	76.6

T.A. = 74.48

*T.A. = Total Accuracy

any two-date combination enhanced corn classification. The effect of adding the third date did nothing to enhance the classification, because no new information was contributed, therefore, the effect was similar to adding noise to the data base.

It has long been recognized that a multidate approach enhances the discrimination of vegetation classes (Goodman, 1959). Analyses of other multitemporal radar data sets have resulted in the same conclusion (Bush and Ulaby, 1977; Ulaby et al., 1979; Brisco and Protz, 1980). However, to be most effective, the multidate approach must consider the data-acquisition period in relation to the crop calendar. The Seasat data used in this analysis were acquired during the harvest period and thus were not optimum for multitemporal crop classification. However, they are the only multitemporal satellite SAR data available, and the results of the present analysis indicate the degree of success that can be expected when using this approach to radar crop classification.

4.6 Multisensor Classification

The category confusion that results from combining the best Seasat date (September 22) with either Landsat band 5 or band 7 is presented in Table 4.5. The classification accuracy (76%) is very similar to that obtained by combining two Seasat dates (75%). As before, wheat is the more accurately classified category, and corn and milo are the most highly confused. Adding one Landsat channel to the two-date Seasat combinations

TABLE 4.5

Category Confusion Tables for the Classifications of September 22 Seasat Data with Landsat Band 5 or Band 7 for Corn (C), Milo (M), and Wheat (W)

	September 22/Band 5		
	C	M	W
C	68.8	30.5	0.8
M	14.1	74.2	11.7
W	0.0	14.8	85.2
	T.A.* = 76.04		

	September 22/Band 7		
	C	M	W
C	69.5	28.1	2.3
M	13.3	65.6	21.1
W	0.8	6.3	93.0
	T.A. = 76.04		

*T.A. = Total Accuracy

that produced the best accuracies in Section 4.4 yields similar classification accuracies to those obtained using the three-date Seasat combination (Table 4.6).

When the Seasat/Landsat combinations were used, corn was the category that showed the most improvement. This was indicated in the single-channel analyses described in Section 4.3. The lower reflections from corn on band 7, combined with the brightest tones on the Seasat images, enabled the multisensor combination to improve corn discrimination. However, some accuracy in milo identification was sacrificed, and hence the total classification accuracies of approximately 75% are quite similar.

Further increases in the number of channels used in the classification added little to the total classification accuracies achieved. Table 4.7 shows the category-confusion tables resulting from the four- and five-channel classifications. The best overall classification accuracy of 78% was achieved using either two Landsat and two Seasat channels or three Seasat channels with Landsat band 5. Wheat remained the most accurately classified crop, with an identification accuracy of approximately 90%. Corn was the next most accurately identified crop, with accuracies exceeding 70%, and in the case of Landsat bands 5 and 7 in combination with Seasat images September 22 and October 1, an identification accuracy of 84% was achieved. Milo was the crop most confused with other categories, with an identification accuracy of approximately 70%. The five-channel classification performed

TABLE 4.6

Category Confusion Tables for the Classifications of September 22 and October 1 or October 7 Seasat Data with Landsat Band 5 and Band 7. Categories are Corn (C), Milo (M), and Wheat (W).

September 22/October 1/Band 5

	C	M	W
C	80.5	19.5	0.0
M	40.6	48.4	10.9
W	3.1	5.5	91.4

T.A.* = 73.44

September 22/October 7/Band 7

	C	M	W
C	74.2	24.2	1.6
M	21.1	69.5	9.4
W	0.8	11.7	87.5

T.A. = 77.08

September 22/October 1/Band 5

	C	M	W
C	65.6	33.6	0.8
M	15.6	77.3	7.0
W	2.3	13.3	84.4

T.A. = 75.78

September 22/October 7/Band 7

	C	M	W
C	75.8	23.4	0.8
M	28.1	62.5	9.4
W	5.5	7.0	87.5

T.A. = 75.26

*T.A. = Total Accuracy

TABLE 4.7

Category Confusion Tables for Four- and Five-Channel Multisensor Classifications of Corn (C), Milo (M), and Wheat (W)

Sept. 22/Oct. 1/Oct. 7/Band 5

	C	M	W
C	73.4	22.7	3.9
M	16.4	71.1	12.5
W	0.0	10.2	89.8

T.A.* = 78.13

Sept. 22/Oct. 1/Oct. 7/Band 7

	C	M	W
C	70.3	28.1	1.6
M	19.5	68.8	11.7
W	3.1	7.8	89.1

T.A. = 76.04

Sept. 22/Oct. 1/Oct. 7/Band 5

	C	M	W
C	84.4	14.8	0.8
M	25.8	60.2	14.1
W	0.8	9.4	89.8

T.A. = 78.13

Sept. 22/Oct. 1/Oct. 7/ Band 7

	C	M	W
C	74.2	25.0	0.8
M	22.7	73.4	3.9
W	2.3	10.2	87.5

T.A. = 78.39

Sept. 22/Oct. 1/Oct. 7/ Band 5/Band 7

	C	M	W
C	71.3	28.8	0.0
M	21.3	66.3	12.5
W	5.0	6.3	88.8

T.A. = 75.47

*T.A. = Total Accuracy

worse than the four-channel combinations, with a total accuracy of 75%. This was attributed to the fifth channel's acting as noise in the classification, because no new information was added to the discrimination.

Previous studies using multisensor combinations for crop identification have shown an increase in classification accuracy when radar and optical data are combined (Ahern et al., 1978; Eyton et al., 1980; Ulaby et al., 1982). The present study has demonstrated that both the multidate and multisensor approaches increase the crop-classification accuracies achieved using MLC. The multidate approach works because of the dynamics of radar backscattering for a given crop over the growing season. The multisensor approach is successful because of the different interaction mechanisms operating between electromagnetic energy and the plant canopy. For example, radar responds to water content and the geometry of the vegetation biomass, whereas band 7 is sensitive to changes in plant cell structure, which is indirectly related to plant water content.

One major limitation of this study was the time period during which the image data were recorded. The late September, early October time frame of the study was coincident with the beginning of the corn and milo harvest. In all likelihood, the high confusion between corn and milo reported above could be reduced by acquiring data during other periods of the crop-growth calendar. For example, it is possible that data taken early in the growing season may be able to discriminate corn from milo because corn is planted at an earlier date and there

will be developmental differences between the crops.

4.7 Summary

Satellite SAR and MSS data were used both alone and in combination to classify corn, milo, and wheat. The best single-channel classification accuracy (67%) was achieved using a September 22 Seasat scene. The classification accuracy was improved to approximately 75% by using either a multidate Seasat combination or Landsat data in a multisensor combination. The overall best classification accuracy of 78% was achieved with a four-channel combination of either Landsat band 5 or band 7 with the Seasat dates.

Table 4.8 presents a summary of many of the crop-classification studies performed using radar data. Although the research described above is the first to use satellite radar data in a multidimensional approach to crop-classification, comparable classification accuracies have been achieved using other methods. Due to the great mix of crop types and sensor characteristics present in these studies, it was difficult to compare results. Nonetheless, the results support the usefulness of radar data as discriminators of crop types.

To achieve classification accuracies either approaching or exceeding 90%, multidate and/or multisensor data are needed. Results reported in the literature to date verify this observation. By evaluating the crop calendar and crop mix of any particular geographic region and using the knowledge gained from previous studies, optimum dates for data acquisition can be

TABLE 4.8

Summary of Crop-Classification Studies Performed Using Radar Data*

Authors	Sensor Parameters Platform	f	P	θ	Crop Types	Classification Accuracy Range (%)
Batlivala and Ulaby (1975)	Aircraft	L	HH HV	60-75°	Corn, soybeans, pasture, woods	65-74
Bush and Ulaby (1978)	Ground-based	KU X	HH HV VV	40-60°	Corn, milo, soybeans wheat, alfalfa	55-90
Ahern et al. (1978)	Aircraft	KU	HH HV	--	Corn, alfalfa, barley cut hay, ripe oats, green pasture, grass, clover and grass, green oats, standing hay, brown pasture	63-85
Ulaby et al. (1979)	Ground-based	KU X	HH VV HV	--	Alfalfa, bare, corn, wheat, milo, soybeans	41-97
Eyton et al.	Ground-based	KU X	VV HV	--	Corn, soybeans, milo	45-82
Goodenough et al. (1980)	Aircraft	X L	HH HV	43° 22°	Potatoes, grains, pasture, fallow, forest	52-73
Shanmugan et al. (1981)	Aircraft	C L	HH HV	10-90°	Corn, wheat stubble, pasture, fallow	57-98
Ulaby et al. (1982)	Aircraft	KU	VV	50°	Corn, wheat stubble, pasture, fallow	61-71
Brisco and Protz (1982)	Aircraft	X L	HH HV	68°	Corn, grain, hay-pasture, roughland, woods	72
Shanmugan et al. (1983)	Aircraft	C L	HH HV	10-50°	Corn, pasture, bare soil	35-98
Brisco et al. (1984)	Aircraft	X L	HH HV	60-65°	Corn, woods, grain, other	83

*Full citations are given in the reference section.

identified. This, in concert with appropriate sensor selection, will allow accurate crop classifications to be made using remotely sensed data.

CHAPTER 5

FOREST MAPPING WITH RADAR

5.1 Introduction

Global forest reserves are rapidly diminishing as a result of the increased demand placed upon wood products by an expanding population. Forests are also being cleared to provide living space and increase agricultural productivity to accommodate a growing populace, especially in developing countries. Thus, it is important to inventory and monitor forest resources on both a regional and a global scale. Remote-sensing techniques have been promoted as a tool useful in meeting this need (Beaubien, 1978; Honer, 1978).

An early study investigating the use of radar imagery for vegetation mapping concluded that vegetation influences upon radar returns were observable in all cases investigated (Morain and Simonett, 1966). Indeed, shortly after this finding was reported, ambitious vegetation-mapping projects were carried out in Brazil (Azevedo, 1971) and Panama (Viksne et al., 1970). Recent studies have investigated the use of radar imagery for more detailed forest mapping and have included information even at the species level (Knowlton and Hoffer, 1981; Krohn et al., 1983; Hoekman, 1984). The results of these studies support the capability of radar to discriminate among forest types in many, but not all, cases.

In Chapters 3 and 4, the use of satellite SAR data both alone and in combination with satellite MSS data was investigated for

land-cover and crop-type classification. In these investigations, image tone, represented by a digital number, was the classifying feature. Results indicated that multidate and/or multisensor data were necessary for accurate classification. According to other studies, texture, another image feature, also can be very useful in radar image interpretation (Berger, 1970; Lowry et al., 1978).

Texture is the spatial distribution of image gray tone for a feature of interest. Although texture has been used successfully to improve classification results with radar data for a variety of applications (Haralick, 1979; Brisco and Protz, 1980; Shanmugan et al., 1981), there has been no consistent method of defining, measuring, or using texture for interpretation and classification. In his article on texture, Haralick (1979) provides a review of the statistical and structural approaches to the uses of texture. He identifies eight statistical approaches to extracting textural information from an image: (1) the autocorrelation function, (2) optical transforms, (3) digital transforms, (4) texture edgeness, (5) the structural element, (6) gray-tone cooccurrence, (7) run lengths, and (8) auto-regressive models.

The present study investigates the use of SIR-A data for forest-type classification. Image tone and texture are used both alone and in combination in a supervised maximum-likelihood classification of broadleaf evergreen (B), broadleaf deciduous (D), needleleaf evergreen (E), and mixed (broadleaf deciduous and needleleaf evergreen) (M) forest types. A grassland-forest transition zone (G), Galeria forest, is also

included as a class. This is a scrub forest like the Cerrados forest type.

5.2 Test-Site and Forest Descriptions

Five forest types were selected for the analyses based on (1) SIR-A coverage and data availability for the type, and (2) variety of forest canopy conditions represented. These criteria resulted in the selection of the sites presented in Figure 5.1. A description of these forests and the SIR-A data-take numbers are listed in Table 5.1. The system parameters for SIR-A were presented in Section 3.1.

The forest types chosen represent the range of canopy conditions expected in wooded areas. They range from the lush, multistoried, many-specied canopy of the tropical forest to the nearly monospecific pine forests of the southeastern United States. The broadleaf deciduous and mixed forests represent intermediate canopy conditions in terms of diversity and productivity. Finally, the Galeria forest of southeastern Brazil represents the transition zone from woody vegetation to grassland, and is characterized by a less dense canopy intermixed with open areas. Figures 5.2 through 5.6 include examples of the five forest classes considered in this analysis as well as the SIR-A data for these forest types.

5.3 Data Analysis

The SIR-A imagery was digitized to 256 gray levels by the Environmental Remote Sensing Center at the University of Wisconsin on a scanning microdensitometer with a 25-μm aperture. This

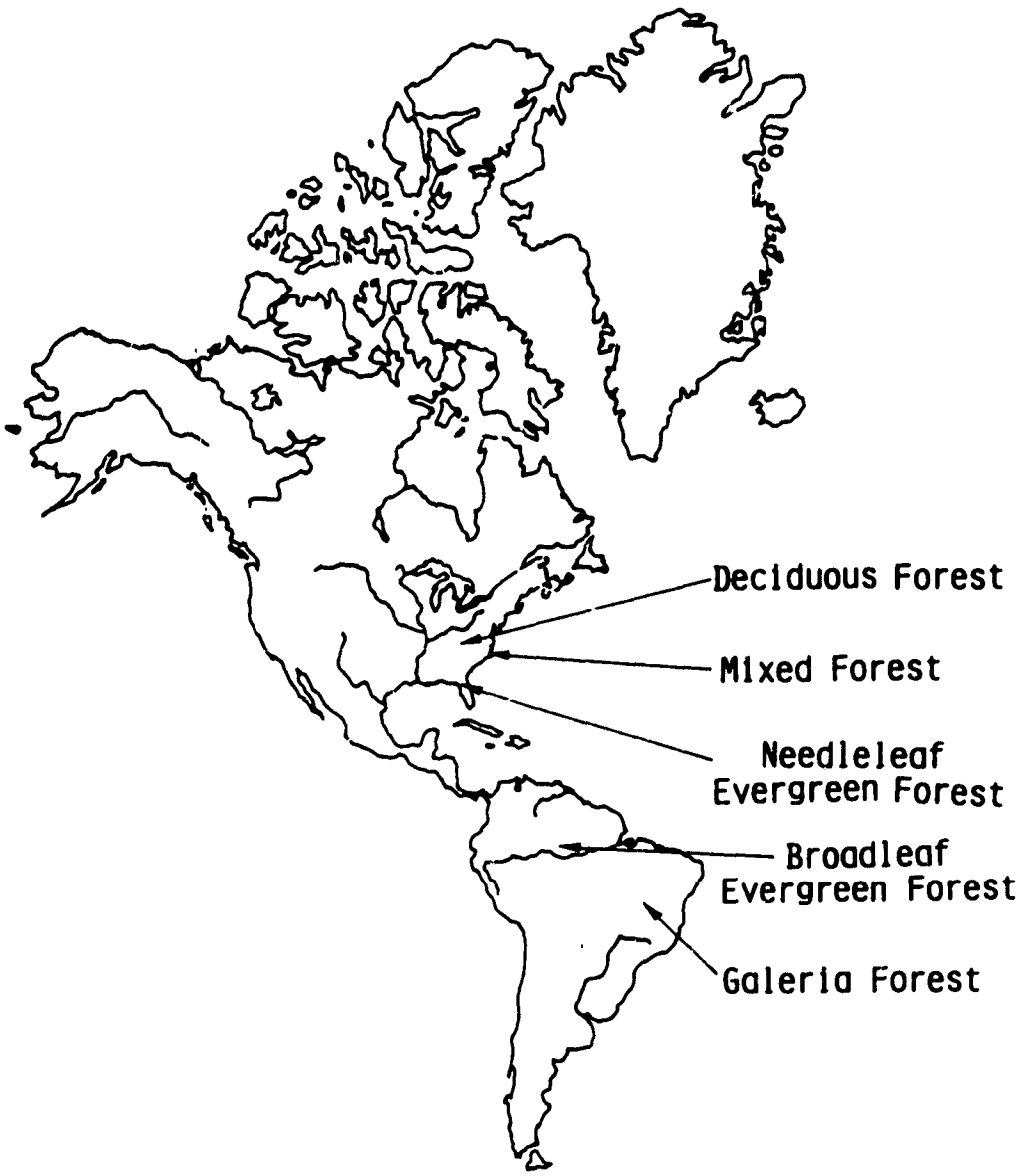

Fig. 5.1. Geographic locations of the five areas used in the selection of the forested regions.

TABLE 5.1

Description of the Five Forest Types and SIR-A Data-Take Numbers Used in this Study. All SIR-A Data Were Acquired on November 13, 1981.

	Site	Forest Type	Symbol	SIR-A Data Take
1)	Amazon Basin	Broadleaf evergreen: tropical rainforest	B	22
2)	Kentucky	Broadleaf deciduous: Oak-Ash-Maple	D	20
3)	North Carolina	Mixed: Oak-Pine	M	20
4)	Alabama	Needleleaf evergreen: Pine	E	21
5)	Brasilia	Galeria forest: grassland, herbaceous plants, and semi-deciduous forest	G	22

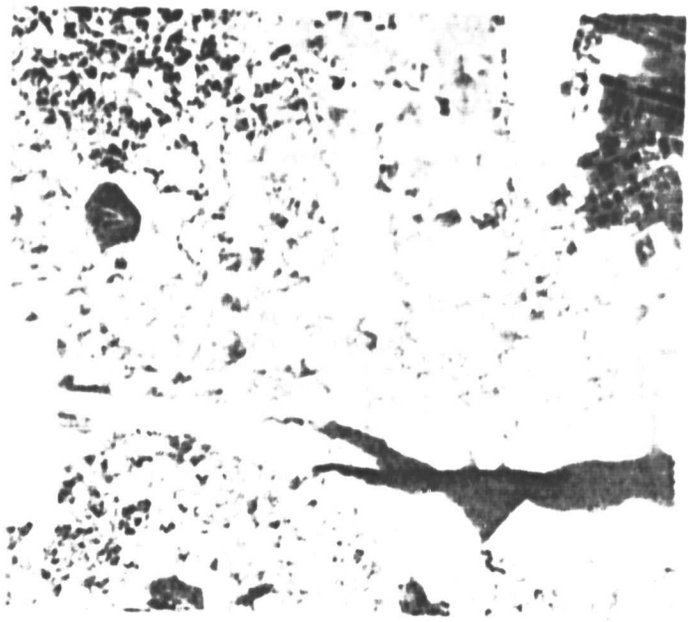

(a)

(b)

Fig. 5.2. (a) SIR-A image of North Carolina and (b) example of the mixed forest (M) category.

(a)

(b)

Fig. 5.3. (a) SIR-A image of central Kentucky and (b) example of the deciduous forest (D) category.

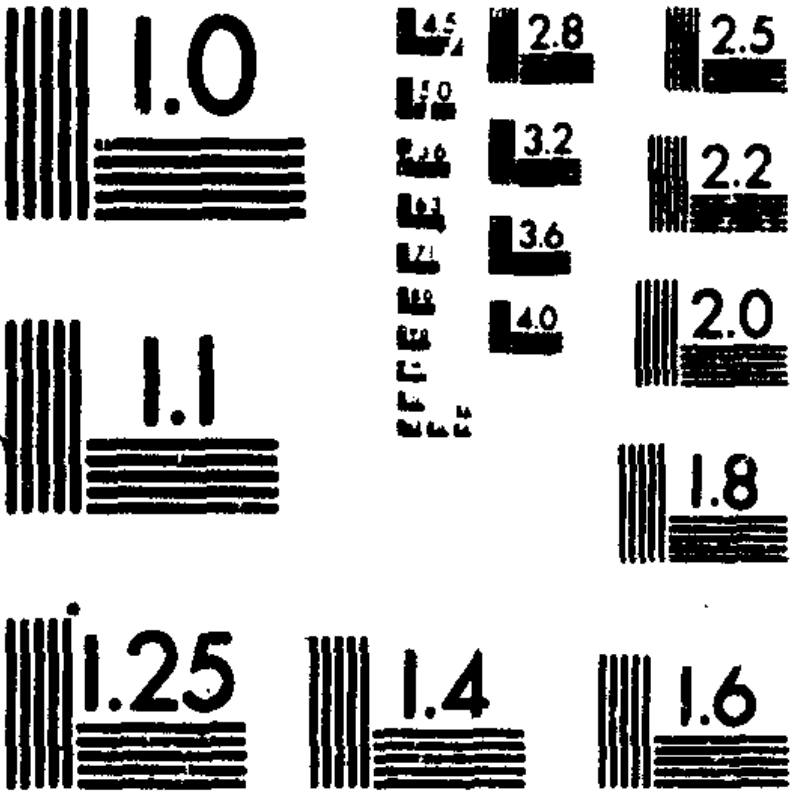

MICROCOPY RESOLUTION TEST CHART
NATIONAL BUREAU OF STANDARDS
STANDARD REFERENCE MATERIAL 1010a
(ANSI and ISO TEST CHART No. 2)

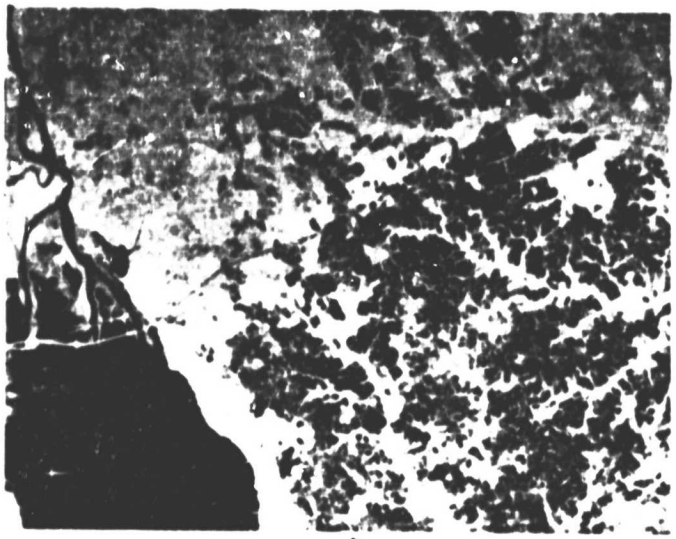

(a)

(b)

Fig. 5.4. (a) SIR-A image of Alabama and (b) example of the coniferous forest (C) category.

C-7

(a)

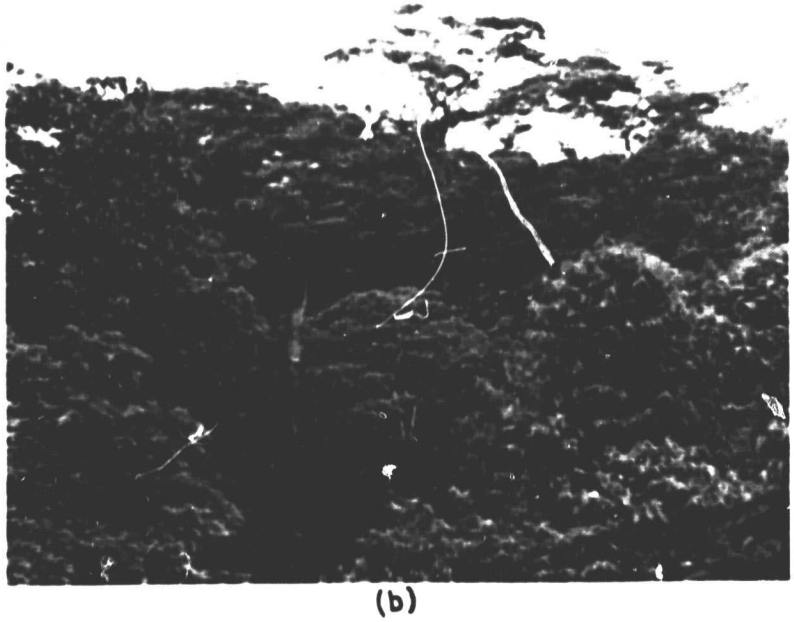

(b)

Fig. 5.5. (a) SIR-A image of central Brazil and (b) example of the broadleaf evergreen (E) category.

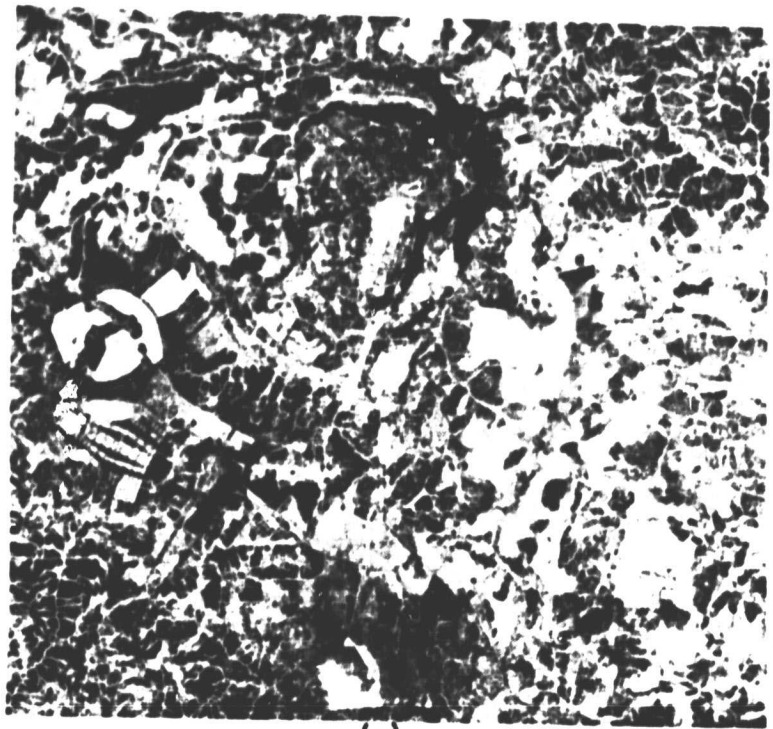

(a)

(b)

Fig. 5.6. (a) SIR-A image of southeastern Brazil and (b) example of the Galeria forest (G) category.

aperture size resulted in an average of 2 x 2 pixels being used for each digital number (DN) value produced. Thus, the SIR-A data were averaged to 24 looks (2 x 2 x 6) with an 80-m x 80-m resolution cell. Fading was significantly reduced by this amount of averaging (Bush and Ulaby, 1975). The data were received in the form of computer-compatible tapes.

The VDI image-analysis system was then used to identify the corner-point coordinates for six 32- x 32-pixel windows for each of the five forestry types. These data were then extracted for subsequent analysis on the University of Kansas Honeywell computer system. An 8-pixel by 8-pixel moving window was used to calculate the local mean and two measures of texture: contrast and inverse moment. Equations 5.1 through 5.3 were used for these calculations.

$$\text{Mean:} \quad \bar{X} = \frac{\sum_{i=1}^{N} X_i}{N} \tag{5.1}$$

$$\text{Contrast:} \quad \sum_{i,j} |i-j|^k (P_{ij})^{\ell} \tag{5.2}$$

$$\text{Inverse Moment:} \quad \sum_{\substack{i,j \\ i \neq j}} \frac{(P_{ij})^{\ell}}{|i-j|^k} \tag{5.3}$$

These textural calculations were based on the gray-tone co-occurrence matrix. This is a matrix of relative frequencies, P_{ij}, with which two neighboring resolution cells separated by distance D occur on the image, one with gray-level i, and the other with gray-level j. All angular relationships (0°, 45°, 90°, 135°) were calculated and then averaged such that directionality did not

enter the interpretation of the results. Haralick (1979) provides a detailed description of this approach to texture calculation. Due to the random nature of vegetation distributions in natural forests and the coarse resolution of the SIR-A data, a distance of 1 between resolution cells, with no directionality, was chosen.

Thus, the preprocessing resulted in 30 data sets, six from each forest type, with each having a 16 x 16 data set representing local mean, contrast, and inverse moment. Histograms of gray level (local mean) and contrast were plotted.

These data were then subjected to supervised maximum-likelihood classification (MLC) using a 20%-training and 80%-testing sample. This was performed separately for tone and then texture as features. Each textural feature was then combined with tone and the two-channel combinations were reclassified. Finally, all three measures were used together in a three-channel classification. All classifications were performed using the MLC algorithm used in previous chapters.

5.4 Results and Discussion

The histograms of gray level and contrast presented in Figure 5.7 and 5.8 allow a preliminary evaluation of the way in which these data will perform in classification analyses. The gray-level histogram (Figure 5.7) indicates good separability for the broadleaf evergreen and broadleaf deciduous forest types. However, there appears to be high confusion among the other three forest categories. Although the Galeria forest was separable using the textural measure of contrast (Figure 5.8), the other

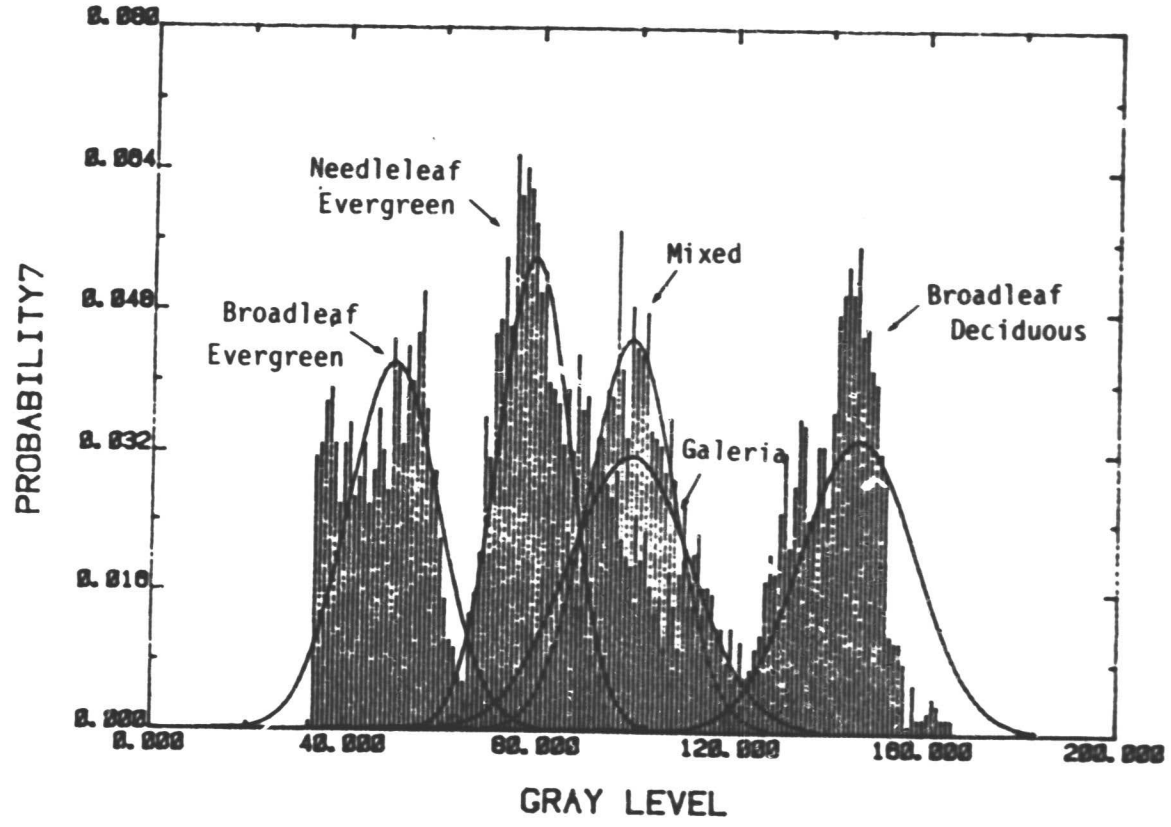

Fig. 5.7. Histograms of gray levels for the five forest categories.

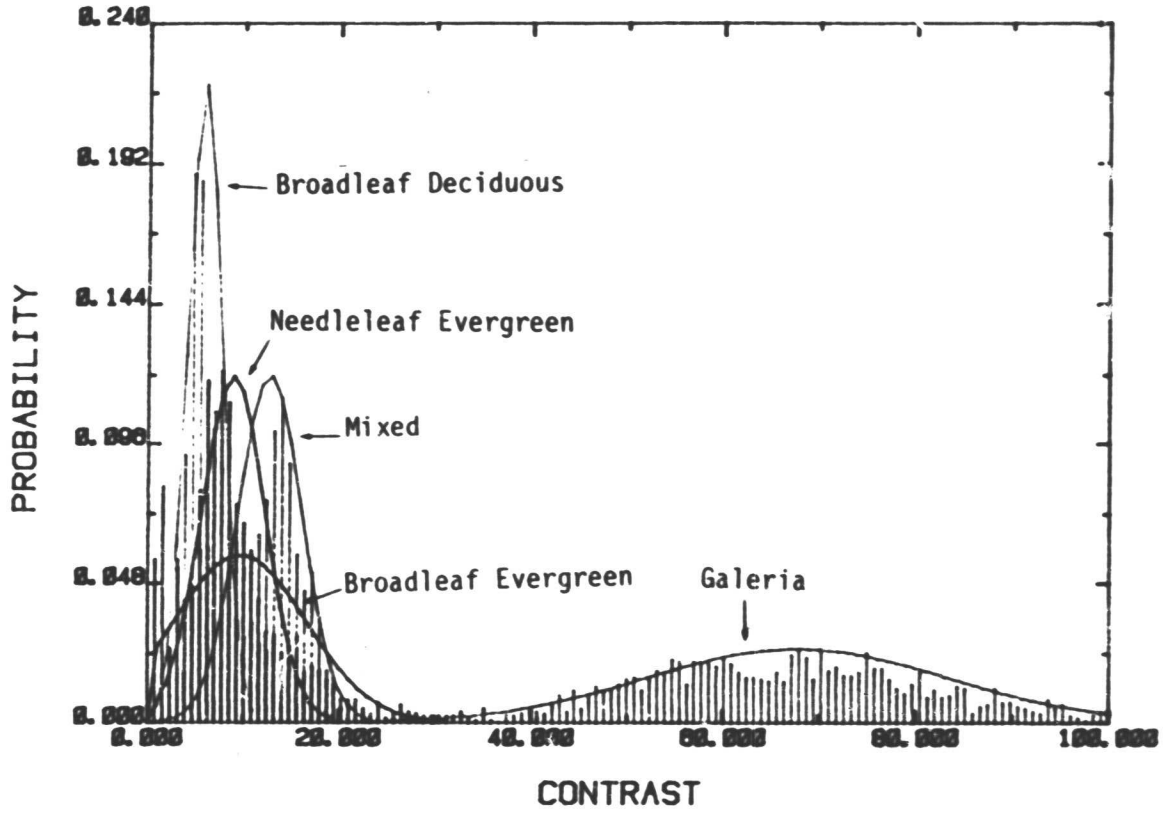

Fig. 5.8. Histograms of contrast for the five forest categories.

four forest categories appeared to be highly confused when texture alone was used.

When gray level was used in a single-channel classification, an accuracy of 75% was achieved (Table 5.2). As indicated by the histograms, broadleaf evergreen and broadleaf deciduous forests are highly separable, with classification accuracies exceeding 95%. The needleleaf evergreen and mixed forest categories were identified accurately 86% and 76% of the time, respectively. The Galeria forest was very poorly classified (17.5%) and was confused primarily with the mixed forest and then with the needleleaf evergreen forest.

Both measures of texture--contrast and inverse moment--produced similar classification accuracies (60% and 57%, respectively; see Tables 5.3 and 5.4). In both classifications, the Galeria forest was highly separable, yielding classification accuracies exceeding 95%. This may have been due to the patchiness of the canopy in this forest category, in which patches of grassland are intermixed with forested areas. The mixed deciduous forest was identified correctly 76% of the time using inverse moment, and with 65% accuracy using contrast. In both cases, it was the needleleaf evergreen category that was most often confused with the mixed deciduous category. The broadleaf deciduous category was classified with 83% accuracy using contrast as the discriminatory feature but only 49% using inverse moment. The needleleaf evergreen and broadleaf evergreen categories were poorly classified by both textural features.

TABLE 5.2

Supervised Maximum-Likelihood Classification of Gray Level Into Forest Categories of Broadleaf Evergreen (B), Broadlead Deciduous (D), Mixed (M), Needleleaf Evergreen (E), and Galeria (G)

True	Classified as (%)				
Category	B	D	M	E	G
B	96.1	0.0	0.0	3.9	0.0
D	0.0	99.2	0.0	0.0	0.8
M	0.0	0.5	76.1	11.0	12.4
E	2.0	0.0	12.1	85.9	0.0
G	0.0	4.2	51.3	26.9	17.5

Overall Accuracy = 74.96%

TABLE 5.3

Supervised Maximum-Likelihood Classification of Contrast Into Forest Categories of Broadleaf Evergreen (B), Broadlead Deciduous (D), Mixed (M), Needleleaf Evergreen (E), and Galeria (G)

True	Classified as (%)				
Category	B	D	M	E	G
B	19.6	35.5	24.3	18.2	2.2
D	0.7	82.8	1.9	14.6	0.0
M	4.3	9.0	65.3	21.4	0.0
E	43.4	2.8	23.6	30.2	0.0
G	0.0	0.0	0.0	0.0	100.0

Overall Accuracy = 59.59%

TABLE 5.4

Supervised Maximum-Likelihood Classification of Inverse Moment Into Forest Categories of Broadleaf Evergreen (B), Broadlead Deciduous (D), Mixed (M), Needleleaf Evergreen (E), and Galeria (G)

True	Classified as (%)				
Category	B	D	M	E	G
B	33.6	33.3	14.7	17.8	0.6
D	12.6	49.0	13.8	24.7	0.0
M	0.0	6.4	76.2	14.2	3.3
E	2.8	29.3	39.3	27.4	1.1
G	0.0	0.0	3.7	0.0	96.3

Overall Accuracy = 56.50%

TABLE 5.5

Supervised Maximum-Likelihood Classification of Gray Level and Contrast into the Forest Categories Broadleaf Evergreen (B), Broadlead Deciduous (D), Mixed (M), Needleleaf Evergreen (E), and Galeria (G)

True	Classified as (%)				
Category	B	D	M	E	G
B	95.3	0.0	0.0	3.5	1.2
D	0.0	99.7	0.3	0.0	0.0
M	0.0	0.0	86.7	13.3	0.0
E	2.4	0.0	12.1	85.5	0.0
G	0.0	0.0	0.0	0.0	100.0

Overall Accuracy = 93.44%

The results of the one-dimensional classification indicate that combining tonal and textural measurements into a multi-dimensional classification may be profitable. This is because it was found that the most accurately identified categories vary with the image feature being used in the classification. As the data in Tables 5.5 through 5.7 reveal, this is indeed the case. The broadleaf evergreen (B), deciduous (D), mixed (M), and needleleaf evergreen (E) classes were separable using image tone as the criterion. Contrast enabled the separation of the Galeria forest (G) from the deciduous (D), and mixed (M) classes, whereas inverse moment separated the G from the M class.

The results were quite similar for both the two-dimensional and the three-dimensional classifications. Approximately 93% of the pixels were accurately identified, with the categories of broadleaf deciduous, broadleaf evergreen, and Galeria forest exhibiting accuracies exceeding 90%. The needleleaf evergreen and mixed forest categories were identified correctly approximately 85% of the time.

At the 80-meter resolution used in this study, each pixel represents only a small number of trees, yet the number and diversity of the trees varies with forest type. For example, a pine forest is likely to contain more trees but fewer species per pixel than a tropical rain forest, which will contain fewer but larger individual trees and more species. Nevertheless, an 80-m resolution may be useful in forest-type classification, since the vegetation-distribution differences between major forest types are likely to be apparent at this scale. This is consistent with the

TABLE 5.6

Supervised Maximum-Likelihood Classification of Gray Level and Inverse Moment into Forest Categories of Broadleaf Evergreen (B), Broadlead Deciduous (D), Mixed (M), Needleleaf Evergreen (E), and Galeria (G)

True	Classified as (%)				
Category	B	D	M	E	G
B	92.8	0.0	0.0	7.1	0.1
D	0.0	99.8	0.2	0.0	0.0
M	0.0	0.1	84.6	12.7	2.6
E	2.4	0.0	11.1	85.6	0.8
G	0.0	0.0	3.7	0.4	95.9

Overall Accuracy = 91.77%

TABLE 5.7

Supervised Maximum-Likelihood Classification of Gray Level, Contrast, and Inverse Moment into the Forest Categories Broadleaf Evergreen (B), Broadlead Deciduous (D), Mixed (M), Needleleaf Evergreen (E), and Galeria (G)

True	Classified as (%)				
Category	B	D	M	E	G
B	93.7	0.0	0.0	5.5	0.8
D	0.0	99.8	0.2	0.0	0.0
M	0.0	0.1	85.7	14.2	0.1
E	3.4	0.0	11.4	85.2	0.0
G	0.0	0.0	0.0	0.0	100.0

Overall Accuracy = 92.89%

mesoscale roughness Morain (1976) describes in his article on radar-image interpretation for vegetation analysis. He defines **microroughness** as gray-tone fluctuations due to frequency, **mesoscale roughness** as the gross roughness envelope directly related to image texture, and **macroscale roughness** as the complex image tone arising out of a combination of micro- and mesoscale roughness superimposed upon sloping terrain.

The SIR-A data from the different sites may contain inherent gray-tone shifts due to both lack of calibration and the presence of signal-power fluctuations during data recording. Thus, a single target may produce different gray tones on two different SIR-A data-takes. Moreover, the presence of gray-tone shifts can critically affect tonal classification, although if the sensitivity (film gamma) is the same, the shifts will have little effect on textural classification. The SIR-A data were processed by the Jet Propulsion Laboratory (JPL), and personnel there were contacted concerning this difficulty. According to JPL, the signal films were all processed with a gamma of 1, and all subsequent image duplicates were processed with a gamma of 1.2. Thus, although gray-tone shifts may indeed be present, the sensitivity of the image should be the same for each pass.

Other researchers have reported success in forest-type classification, in some cases ranging in detail to the species level, using multiparameter radar data (Shuchman et al., 1978; Churchill and Keech, 1983; Knowlton and Hoffer, 1981; Hoekman, 1984). Krohn et al. (1983) also reported some success at discriminating upland from lowland forest types on the East Coast,

using Seasat data. Graf and Rode (1982) reported moisture-dependent effects in the backscattering from the branches and leaves of a fir tree. Bush et al. (1976) described temporal variation in the canopy backscattering from a deciduous forest. These observations lend further credence to the use of microwave remote sensing in forest mapping and monitoring.

Further research into and development of space-SAR technology undoubtedly will hasten the operational use of radar data and will ultimately allow foresters to benefit from the technology in practical ways. Space-SAR data, both alone and in combination with MSS data, will prove useful for a wide variety of tasks from simple mapping projects to more elaborate monitoring and disease-control projects.

5.5 Summary

SIR-A data were classified into the forest categories broadleaf evergreen (B), broadleaf deciduous (D), mixed (M), needleleaf evergreen (E), and Galeria forest (G), using maximum-likelihood techniques. Tone (gray level) outperformed textural measures (inverse moment and contrast) as a one-dimensional classifier, producing a classification accuracy of 75% compared to 55-60% for textural-feature classification. Tone was the most useful discriminant for the B, D, M, and E forest categories. The Galeria forest (G) was the most successfully discriminated category on the basis of the textural features. This success was attributed to the patchiness of the canopy for the Galeria class when compared to the other classes. However, combining tone and

texture into a multidimensional classification method resulted in overall classification accuracies exceeding 90%. The multidimensional approach also may be useful in other forest research projects using SAR data, and this possibility should be investigated.

All three studies used a multidimensional approach to land-cover classification. The available uncalibrated SAR data were acquired during less-than-optimum time periods, i.e., late in the growing season, and were generally accompanied by poor ground-truth information. These limitations reduced the scope of the conclusions reached by this investigation. Furthermore, at the time of this study, only two spaceborne SARs had been used; as a result, few data were available to support investigations of this nature. Recently, SIR-B was carried aboard a Shuttle flight and acquired the first space-SAR data with variable incidence angles. Plans have also been made for a C- and L-band radar in the near future, also to be carried aboard the Shuttle as part of the SIR-C experiment. The European Space Agency (ESA) and countries such as Canada and Japan also plan future space-SAR systems. Thus, it appears that quality space-SAR data will become available in the near future.

When timely, calibrated data become available, further research should be carried out to increase both our understanding and utilization of SAR data. For example, critical time periods for data collection can be identified, depending upon the application being investigated. Many of the results reported in this manuscript, and in the literature in general, point to the importance of phenological differences in the discrimination of vegetation types. An excellent example of the importance of phenological differentiation is the success of radar operating at L-band frequencies in discriminating corn from forests early in the growing season; as the season progresses, however, the two

cover types become confused.

Given an understanding of the temporal pattern of radar backscattering, the complemcntary nature of the different wavelengths (optical and microwave) should be studied further. This will enable the efficient use of the data available for each particular task. For example, only one frequency in each of the radio bands and in the optical region may be needed to accurately identify land use at a Level I differentiation. However, for Level II characterization, many channels, selected from the range of wavelengths available, may be necessary.

Texture analysis is a promising approach to the utilization of remote-sensing data. As the algorithms become available for incorporating texture measurements into digital classifications, the information content available from radar data will undoubtedly increase. Texture has been recognized as an important element in radar-image interpretation but has been difficult to incorporate into machine classification. Progress is being made in this area, and the future appears promising.

The multidimensional approach is indicative of the direction remote sensing must take in order to meet some of the goals for which it is being evaluated. One must choose an approach that is both cost-effective and meets the requirements of the particular task being undertaken. A single-date acquisition and subsequent digital classification using tone and/or texture may be sufficient for some purposes--for example, mapping the extent of flooding after severe storms. More complex problems, such as monitoring agricultural productivity, will probably require multisensor data

as well as multidate acquisitions. Digital pre- and post-processing requirements will thus be extensive, which will also add significantly to both the cost and effort required. The information produced must be of considerable value to warrant such an undertaking.

One satellite system, Landsat-5, with its MSS and TM sensors, is entering a new era as an operational system. Research is now being conducted to bring microwave remote-sensing to a similar status. With a truly operational SAR system in space, the number and complexity of the tasks that can be accomplished by remote-sensing technology will increase.

Land-cover classification will be possible at detailed levels of discrimination. This will enable both the accurate identification of and tabulation of land-use dynamics, which will become increasingly important as population pressure increases. Improved yield estimations and disease monitoring will also allow better utilization of renewable resources. It thus appears that remote sensing will be an indispensable tool for the resource manager of the future.

REFERENCES

Ahern, F. J., D. G. Goodenough, A. L. Grey, R. A. Ryerson, and R. J. Vilbikaitis (1978), "Simultaneous Microwave and Optical Wavelength Observations of Agricultural Targets, Can. J. Remote Sensing, Vol. 4, No. 2, pp. 127-142.

Anderson, J. R., E. E. Hardy, J. T. Roach, and R. E. Witner (1976), "A Land Use and Land Cover Classification System for Use with Remote Sensor Data," United States Geological Survey Circular 671, United States Printing Office, Washington, DC.

Azevedo, L. A. H. (1971), "Radar in the Amazon," Proc. 7th Int. Symp. Remote Sensing of Environment, Univ. of Michigan, Ann Arbor, May 17-21, Vol. 3.

Batlivala, P. P., and F. T. Ulaby (1975), "Crop Identification from Radar Imagery of the Huntington County, Indiana Test Site," RSL Tech. Rep. 177-58, Remote Sensing Laboratory, Univ. of Kansas Center for Research, Inc., Lawrence, KS.

Batlivala, P. P., and F. T. Ulaby (1976a), "Radar Look Direction and Row Crops," Photogram. Eng. and Remote Sensing, Vol. 42, No. 2, pp. 233-238.

Batlivala, P. P., and F. T. Ulaby (1976b), "Feasibility of Monitoring Soil Moisture Using Active Microwave Remote Sensing," RSL Tech. Rep. 264-12, Remote Sensing Laboratory, Univ. of Kansas Center for Research, Inc., Lawrence, KS.

Bauer, M. E. (1975), "The Role of Remote Sensing in Determining the Distribution and Yield of Crops," Advances in Agriculture, Vol. 27, pp. 271-304.

Beaubien, J. (1978), "Forest Type Mapping from Satellites Six Years After," Proc. 5th Canadian Symp. on Remote Sensing, Victoria, British Columbia, August, pp. 43-58.

Berger, D. H. (1970), "Texture as a Discriminant of Crops on Radar Imagery," IEEE Trans. Geosci. Electron., Vol. GE-8, No. 4, pp. 334-348.

Bradley, G. A., and F. T. Ulaby (1980), "A Comparison of Ground and Airborne Remote Sensing Radar Measurements," RSL Tech. Rep. 460-1, Remote Sensing Laboratory, Univ. of Kansas Center for Research, Inc., Lawrence, KS.

Brisco, B., and R. Protz (1980), "Corn Field Identification Accuracy Using Airborne Radar Imagery," Can. J. Remote Sensing, Vol. 6, No. 1, pp. 15-24.

Brisco, B., and R. Protz (1982), "Manual and Automatic Crop Identification with Airborne Radar Imagery," Photogram. Eng. and Remote Sensing, Vol. 48, No. 1, pp. 101-109.

Brisco, B., F. T. Ulaby, and R. Protz (1984), "Improving Crop Classification through Attention to the Timing of Airborne Radar Acquisitions," Photogram. Eng. and Remote Sensing, Vol. 50, No. 6, pp. 739-745.

Bryan, M. L. (1975), "Interpretation of an Urban Scene Using Multi-Channel Radar Imagery," Remote Sensing of Environment, Vol. 4, No. 1, pp. 49-66.

Bush, T. F., and F. T. Ulaby (1975), "On the Feasibility of Monitoring Croplands with Radar," Proc. 10th Int. Symp. Remote Sensing of Environment, Univ. of Michigan, Ann Arbor, October.

Bush, T. F., and F. T. Ulaby (1977), "Crop Inventories with Radar," Proc. Remote Sensing and Technol. Symp., Ottawa, Ontario, Canada, February 21-23, pp. 1-17.

Bush, T. F., and F. T. Ulaby (1978), "An Evaluation of Radar as a Crop Classifier," Remote Sensing of Environment, Vol. 7, pp. 15-36.

Bush, T. F., F. T. Ulaby, T. Metzler, and H. Stiles (1976), "Seasonal Variations of the Microwave Scattering Properties of Deciduous Trees as Measured in the 1-18 GHz Spectral Range," RSL Tech. Rep. 177-60, Remote Sensing Laboratory, Univ. of Kansas Center for Research, Inc., Lawrence, KS.

Churchill, P. N., and M. A. Keech (1983), "S.A.R. Investigation of the Thetford Forest," European SAR-580 Experiment, European Space Agency, Paris, France.

Cihlar, J. (1979), "Active Remote Sensing of Agricultural Targets: An Overview," presented at the Agricultural Workshop of the SURSAT Project, January 30, Ottawa, Canada.

Coiner, J. C., (1972), "SLAR Image Interpretation Keys for Geographic Analysis," RSL Tech. Rep. 177-19, Remote Sensing Laboratory, Univ. of Kansas Center for Research, Inc., Lawrence, KS.

de Loor, G. P. (1969), "Possibilities and Uses of Radar and Thermal Infrared Systems," Photogrammetria, Vol. 24, pp. 43-58.

de Loor, G. P., and A. A. Jurriens (1971), "The Radar Backscatter of Vegetation," Proc. AGARD Conf. No. 90, Propagation Limitations of Remote Sensing, North Atlantic Treaty Organization (NATO), CP-90-71, October, Colorado Springs.

de Loor, G. P., A. A. Jurriens, and H. Gravesteijn (1974), "The Radar Backscatter from Selected Agricultural Crops," IEEE Trans. Geosci. Electron., Vol. GE-12, No. 2, pp. 70-74.

Drake, B. (1977), "Necessity to Adapt Land Use and Land Cover Classification Systems to Readily Accept Radar Data," Proc. 11th Int. Symp. Remote Sensing of Environment, Univ. of Michigan, Ann Arbor, April 25-29.

Elachi, C. (1982), "The Shuttle Imaging Radar (SIR-A) Sensor and Experiment," Digest 2nd IEEE Int. Geosci. Remote Sensing Symp. (IGARSS '82), Vol. II, Munich, FRG, June 1-4 (IEEE Cat. No. 82CH14723-6).

Ellermeier, R. D., D. S. Simonett, and L. F. Dellwig (1967), "The Use of Multi-Parameter Radar Imagery for the Discrimination of Terrain Characteristics," RSL Tech. Rep. 61-19, Remote Sensing Laboratory, Univ. of Kansas Center for Research, Inc., Lawrence, KS.

Estes, J. E., and D. S. Simonett (1975), "Image Interpretation," Ch. 14 in Manual of Remote Sensing (1st ed.), R. G. Reeves, Ed., Falls Creek, VA: American Society of Photogrammetry, pp. 869-1072.

Eyton, J. R., R. Li, and F. T. Ulaby (1979), "Combined Radar and Landsat Multitemporal Crop Classification," RSL Tech. Rep. 360-10, Remote Sensing Laboratory, Univ. of Kansas Center for Research, Inc., Lawrence, KS.

Gimbarzevsky, P. (1978), "Land Classification as a Base for Integrated Inventories of Renewable Resources," Proc. of Workshop on Integrated Inventories of Renewable Natural Resources, Tucson, AZ, January.

Goodman, M. (1959), "A Technique for the Identification of Farm Crops on Aerial Photographs," Photogram. Eng. and Remote Sensing, Vol. 28, pp. 984-990.

Graf, G., and B. Rode (1982), "Radar Scattering from a Solitary Fir Tree," Digest 2nd IEEE Int. Geosci. Remote Sensing Symp. (IGARSS '82), Vol. II, Munich, FRG, June 1-4 (IEEE Cat. No. 82CH14723-6).

Haralick, R. M. (1979), "Statistical and Structural Approaches to Texture," Proc. IEEE, Vol. 67, No. 5.

Haralick, R. M., F. Caspall, and D. S. Simonett (1970), "Using Radar Imagery for Crop Discrimination--A Statistical and Conditional Probability Study," Remote Sensing of Environment, Vol. 1, pp. 131-142.

Hardy, N. E. (1972), "Interpretation of Side-Looking Airborne Radar Vegetation Patterns: Yellowstone National Park," RSL Tech. Rep. 177-24, Remote Sensing Laboratory, Univ. of Kansas Center for Research, Inc., Lawrence, KS.

Harris, G. H., and L. C. Graham (1976), "LANDSAT--Radar Synergism," Proc. XIII Congress Int. Soc. Photogrammetry, Helsinki, Finland.

Henderson, F. M. (1975), "Radar for Small-Scale Land-Use Mapping," Photogram. Eng. and Remote Sensing, Vol. 41, pp. 307-319.

Henderson, F. M. (1979), "Land-Use Analysis of Radar Imagery," Photogram. Eng. and Remote Sensing, Vol. 45, pp. 295-307.

Henderson, F. M., S. W. Wharton, and D. L. Toll (1980), "Preliminary Results of Mapping Urban Land Cover with SEASAT SAR Imagery," ACSM-ASP Convention, American Society of Photogrammetry, St. Louis, MO, March 9-14, pp. 310-317.

Hoekman, D. H. (1984), "Radar Backscattering of Forest Parcels," Proc. Int. Symp. Microwave Signatures in Remote Sensing, Toulouse, France, January 16-20.

Honer, T. G. (1978), "The National Shame of Canada's Forest Resource Statistics," Proc. 5th Can. Symp. Remote Sensing, Victoria, British Columbia, August, pp. 1-6.

Intera, Environmental Consultants, Ltd. (1980), "The Airborne SAR Project," Intera Rep. ASP-80-1, Ottawa, Canada.

Jensen, H., L. C. Graham, L. Porcello, and E. Leith (1977), "Side-Looking Airborne Radar," Scientific American, Vol. 23, No. 4, pp. 84-95.

Jordan, R. L. (1980), "The Seasat-A Synthetic Aperture Radar System," IEEE J. Oceanic Eng., Vol. OE-5, No. 2, pp. 154-164.

King, G. J. (1979), "The Crop Information System: A Review," Seminar on Crop Information Systems; Commodity Market Analysis Division; Policy, Planning and Economics Branch; Agriculture Canada, January 23, Ottawa, Canada.

Knowlton, D. J., and R. M. Hoffer (1981), "Radar Imagery for Forest Cover Mapping," Proc. 7th Int. Symp. Machine Proc. Remotely Sensed Data, Purdue Univ., W. Lafayette, IN, June 23-26, pp. 626-632.

Krohn, M. D., N. M. Milton, and D. B. Segal (1983), "Seasat Synthetic Aperture Radar (SAR) Response to Lowland Vegetation Types in Eastern Maryland and Virginia," J. Geophys. Res., Vol. 88, No. C3, pp. 1937-1952.

LACIE Symposium (1978), Proc. Plenary Session, Lyndon B. Johnson Space Center, Houston, TX.

Larsen, R. W., P. L. Jackson, R. J. Dallaire, R. Shuchman, and R. Rawson (1975), "Interpretation and Measurement of Multichannel Microwave SAR Imagery, Proc. 10th Int. Symp.

Remote Sensing of Environment, Vol. 1, Univ. of Michigan, Ann Arbor, October 6-10, pp. 53-69.

Lewis, A. J. (1968), "Evaluation of Multiple Polarized Radar Imagery for the Detection of Selected Cultural Features," RSL Tech. Rep. 61-20, Remote Sensing Laboratory, Univ. of Kansas Center for Research, Inc., Lawrence, KS.

Lewis, A. J., H. C. MacDonald, and D. . Simonett (1969), "Detection of Linear Cultural Features with Multipolarized Radar Imagery," Proc. 6th Int. Symp. Remote Sensing of Environment, Vol. 2, Univ. of Michigan, Ann Arbor, October 13-16.

Lowry, R. T., S. Shlein, and D. G. Goodenough (1978), "A CCRS System for Synthetic Aperture Radar Imagery Analysis," Proc. 5th Can. Symp. Remote Sensing, Victoria, British Columbia, August, pp. 363-372.

Moore, R. K. (1975), "Microwave Remote Sensors," in Manual of Remote Sensing (1st ed.), R. G. Reeves, Ed., Falls Church, VA.: American Society of Photogrammetry, pp. 399-538.

Moore, R. K. (1978), "Active Microwave Sensing of the Earth's Surface--A Mini-Review," IEEE Trans. Antennas and Propag., Vol. AP-26, No. 6, pp. 843-849.

Morain, S. A., and D. S. Simonett (1967), "K-Band Radar in Vegetation Mapping," RSL Tech. Rep. 61-23, Remote Sensing Laboratory, Univ. of Kansas Center for Research, Inc., Lawrence, KS; also appearing in Photogram. Eng. and Remote Sensing, Vol. 33, No. 7, pp. 730-740.

Morain, S. A. (1976), "Use of Radar for Vegetation Analysis in Remote Sensing," Ch. 4 in ElectroMagnetic Spectrum, Vol. 3, pp. 61-78.

Parashar, S., D. Day, J. Ryan, D. Strong, and R. Worsfold (1979), "Radar Discrimination of Crops," Proc. 13th Int. Symp. Remote Sensing of Environment, Vol. II, Univ. of Michigan, Ann Arbor, April 23-27.

Paris, J. (1982), "Radar Remote Sensing of Crops," Digest 2nd IEEE Int. Geosci. Remote Sensing Symp. (IGARSS '82), Vol. II, Munich, FRG, June 1-4 (IEEE Cat. No. 82CH1472-6).

Prout, N. A. (1980), "Land Use/Cover Mapping for Halifax County: Remote Sensing Alternatives," Proc. 6th Can. Symp. on Remote Sensing, Halifax, New Brunswick, May, pp. 307-320.

Rubec, C. D., and J. Cihlar (1980), "Airborne Radar Imagery for Ecological and Land Use/Cover Classification in Canada," Interpreter Evaluations in Intera, ASP-80-1, Ottawa, Canada.

Schwarz, D. E., and F. C. Caspall (1968), "Use of Radar in the Discrimination and Identification of Agricultural Land Use, Proc. 5th Int. Symp. Remote Sensing of Environment, Univ. of Michigan, Ann Arbor, pp. 233-248.

Shanmugam, K. S., V. Narayanan, V. S. Frost, J. A. Stiles, and J. C. Holtzman (1981), "Textural Features for Radar Image Analysis," IEEE Trans. Geosci. Remote Sensing, Vol. GE-19, pp. 153-156.

Shanmugam, K. S., F. T. Ulaby, V. Narayanan, and C. Dobson (1983), "Crop Classification Using Multidate/Multifrequency Radar Data," submitted to Remote Sensing of Environment.

Shuchman, R. A., R. B. Innes, C. L. Liskow, B. T. Larrowe, and A. Klooster (1978), "ERIM Seasat SAR Engineering Evaluation," Univ. of Michigan, Ann Arbor, EM-79-1024.

Simonett, D. S., J. R. Eagleman, A. B. Erhart, D. C. Rhodes, and D. F. Schwarz (1967), "The Potential of Radar as a Remote Sensor in Agriculture. 1. A Study with K-Band Imaging in Western Kansas," RSL Tech. Rep. 61-21, Remote Sensing Laboratory, Univ. of Kansas Center for Research, Inc., Lawrence, KS.

Swain, P. H., and S. M. Davis (1978), Remote Sensing: The Quantitative Approach, New York: McGraw-Hill.

Ulaby, F. T. (1975), "Radar Response to Vegetation," IEEE Trans. Antennas and Propag., Vol. AP-23, No. 1, pp. 36-45.

Ulaby, F. T., and J. E. Bare (1979), "Look Direction Modulation Function of the Radar Backscattering Coefficient of Agricultural Fields," Photogram. Eng. and Remote Sensing, Vol. 45, No. 11, pp. 1495-1506.

Ulaby, F. T., and P. P. Batlivala (1976), Diurnal Variations of Radar Backscatter from a Vegetation Canopy," IEEE Trans. Antennas Propag., Vol. AP-24, No. 1, pp. 11-17.

Ulaby, F. T., and G. Burns (1977), "The potential Use of Radar for Crop Classification and Yield Estimation," Proc. Microwave Remote Sensing Symp., Houston, TX, December 7.

Ulaby, F. T., and T. F. Bush (1975), "Corn Growth as Monitored by Radar," RSL Tech. Rep. 177-57, Remote Sensing Laboratory, Univ. of Kansas Center for Research, Inc., Lawrence, KS.

Ulaby, F. T., and T. F. Bush (1976), "Monitoring Wheat Growth with Radar," Photogram. Eng. and Remote Sensing, Vol. 42, No. 4, pp. 557-568.

Ulaby, F. T., and R. K. Moore (1973), "Radar Spectral Measurements of Vegetation," CRES Tech. Rep. 177-40, Univ. of Kansas Center for Research, Inc., Lawrence, KS.

Ulaby, F. T., T. F. Bush, and H. Stiles (1977), "Space Radar System Specifications," Proc. 11th Int. Symp. Remote Sensing of Environment, Univ. of Michigan, Ann Arbor, April 25-19.

Ulaby, F. T., M. C. Dobson, and G. A. Bradley (1981), "Radar Reflectivity of Bare and Vegetation-Covered Soil," Advanced Space Res., Vol. 1, pp. 91-104.

Ulaby, F. T. R. Eyton, R. Y. Li, and F. F. Burns (1979), "Annual Repeatibility of Multidate Radar Crop Classifications," RSL Tech. Rep. 360-1, Remote Sensing Laboratory, Univ. of Kansas Center for Research, Inc., Lawrence, KS.

Ulaby, F. T., R. Y. Li, and K. S. Shanmugan (1981), "Crop Classification by Radar," RSL Tech. Rep. 360-13, Remote Sensing Laboratory, Univ. of Kansas Center for Research, Inc., Lawrence, KS.

Ulaby, F. T., R. Y. Li, and K. S. Shanmugan (1982), "Crop Classification Using Airborne Radar and Landsat Data," IEEE Trans. Geosci. Remote Sensing, Vol. GE-20, No. 1, pp. 42-51.

Ulaby, F. T., R. K. Moore, and A. K. Fung (1981), Microwave Remote Sensing; Active and Passive, Vol. 1, Reading, MA: Addison-Wesley.

Viskne, A. T., C. Liston, and C. D. Sapp (1970), "SLR Reconnaissance of Panama," Photogram. Eng. and Remote Sensing, Vol. 36, No. 3, pp. 253-259.

Waite, W. P., and H. C. MacDonald (1971), "Vegetation Penetration with K-Band Imaging Radars," IEEE Trans. Geosci. Electron., Vol. GE-9, pp. 147-155.

Wu, S. T. (1980), "An Improvement in Land Cover Classification Achieved by Merging Microwave Data with Landsat Multispectral Scanner Data," ASCM-ASP Convention, American Society of Photogrammetry, St. Louis, MO, March, pp. 293-309.

Zobrist, A. L., R. J. Blackwell, and W. D. Stromberg (1979), "Integration of Landsat, Seasat, and Other Geo-Data Sources," Proc. 13th Int. Symp. Remote Sensing of Environment, Vol. 1, Univ. of Michigan, Ann Arbor.